HHS Public Access

Author manuscript

J Mol Med (Berl). Author manuscript; available in PMC 2018 May 01.

Published in final edited form as:

J Mol Med (Berl). 2017 May ; 95(5): 535–552. doi:10.1007/s00109-017-1506-8.

Targeting The Tight Junction Protein, Zonula Occludens-1, With The Connexin 43 Mimetic Peptide, αCT1, Reduces VEGF-Dependent RPE Pathophysiology

Elisabeth Obert[1], **Randy Strauss**[2], **Carlene Brandon**[1], **Christina Grek**[3], **Gautam Ghatnekar**[3], **Robert Gourdie**[2], and **Bärbel Rohrer**[1,4,5,*]

[1]Department of Neurosciences, Medical University of South Carolina, Charleston, SC 29425

[2]Center for Heart and Regenerative Medicine, Virginia Tech Carilion Research Institute, Roanoke, VA, 24016

[3]FirstString Research Inc. Mount Pleasant, SC 29464

[4]Department of Ophthalmology, Medical University of South Carolina, Charleston, SC 29425

[5]Ralph H. Johnson VA Medical Center, Charleston, SC 29401

Abstract

A critical target tissue in age-related macular degeneration (AMD) is the retinal pigment epithelium (RPE), which forms the outer blood-retina barrier (BRB). RPE-barrier dysfunction might result from attenuation/disruption of intercellular tight junctions. Zonula occludens-1 (ZO-1) is a major structural protein of intercellular junctions. A connexin43-based peptide mimetic, αCT1 was developed to competitively block interactions at the PDZ2 domain of ZO-1, thereby inhibiting ligands that selectively bind to this domain. We hypothesized that targeting ZO-1 signaling using αCT1 would maintain BRB integrity and reduce RPE pathophysiology by stabilizing gap- and/or tight-junctions. RPE-cell barrier dysfunction was generated in mice using laser-photocoagulation triggering choroidal neovascularization (CNV), or bright-light exposure leading to morphological damage. αCT1 was delivered via eyedrops. αCT1 treatment reduced CNV development and fluid leakage as determined by optical coherence tomography, and damage was correlated with disruption in cellular integrity of surrounding RPE cells. Light-damage significantly disrupted RPE cell morphology as determined by ZO-1 and Occludin staining and tiling pattern analysis, which was prevented by αCT1 pre-treatment. *In vitro* experiments using RPE and MDCK monolayers indicated that αCT1 stabilizes tight junctions, independent of its

*Corresponding author: Department of Ophthalmology, Medical University of South Carolina, 167 Ashley Avenue, Charleston, SC 29425; phone: (843) 792-5086; fax (843) 792-1723; rohrer@musc.edu.

AUTHOR CONTRIBUTIONS

Elisabeth Obert: performed experiments and analyzed data.
Randy Strauss: performed experiments and analyzed data.
Carlene Brandon: performed experiments and analyzed data.
Christina Grek: contributed reagents and contributed to the writing of the manuscript.
Gautam Ghatnekar: contributed reagents and contributed to the writing of the manuscript.
Robert Gourdie: contributed to designing the study, contributed reagents and contributed to the writing of the manuscript.
Bärbel Rohrer: designed the study, analyzed data and took the lead in writing the manuscript.

COMPETING INTERESTS

EO and RV have no financial or non-financial competing interests to disclose.

effects on Cx43. Taken together, stabilization of intercellular junctions by αCT1 was effective in ameliorating RPE dysfunction in models of AMD-like pathology.

Keywords

retinal pigment epithelium; connexin43; tight junctions; choroidal neovascularization; light damage; vascular endothelial growth factor; age-related macular degeneration

INTRODUCTION

Age-related macular degeneration (AMD) is a multifactorial disease regarded as the most common cause of central vision loss in the elderly in industrialized countries [1, 2]. In late AMD, patients exhibit damage to the macula, which can occur due to consequences of geographic atrophy (GA) or choroidal neovascularization (CNV). In GA, the RPE degenerates, leading to a progressive loss of photoreceptors. Wet AMD is characterized by the growth of new blood vessels (choroidal neovascularization, CNV) that break through the blood-retina barrier and grow into the retina under the macula. These blood vessels tend to be fragile and often leak blood and fluid. RPE damage and loss of blood-retina barrier function is a common feature in both dry and wet AMD, where the pro-angiogenic factor, vascular endothelial growth factor (VEGF), plays a key pathogenic role [3].

The RPE is composed of a single layer of hexagonal, highly pigmented cells located between the retina and the choroid and forms part of the blood-retina barrier. Its many functions include: transport of molecules between the subretinal space and the choroidal blood supply; spatial ion buffering; secretion of growth factors, proteases, etc., that control the stability of photoreceptors, BrM and the choroid; modulation of the immune response [4] and subretinal fluid resorption [5]. The RPE exhibits three kinds of intercellular junctions: tight, adherens and gap junctions. Tight junctions form a gate or barrier that regulates the paracellular diffusion of solutes and nutrients in the RPE [6]. Adherens junctions provide strong mechanical attachment between adjacent RPE cells; whereas gap junctions allow for cell-to-cell communication within the RPE monolayer.

The connexin subunit of gap junction channels is a tetraspan transmembrane protein. Twenty-one connexin isoforms have been identified in the human genome, each with distinct spatial and temporal expression patterns [7]. The RPE expresses connexin43 (Cx43) and connexin46 (Cx46) [8]. Six connexins assemble into one connexon (hemichannel), while two connexons from adjacent cells dock to form a gap junction channel – the gap junction itself is an aggregate of such channels. Various heteromeric configurations of different connexin proteins can assemble into connexon hemichannels, leading to gap junctions with distinctive communication properties [8]. Tight junctions contain at least 40 proteins,[9] some of which are transmembrane and mediate intercellular adhesion; whereas others are intracellular scaffold proteins that link junctional components to the cytoskeleton. The adhesive elements of adherens junctions are cadherin receptors that bridge the gap between neighboring cell membranes through homophilic interactions. In adherens junctions, catenins are the main scaffolding proteins that tether the mechanical junctions to the cytoskeleton [10].

Zonula occludens-1 (ZO-1) is a scaffolding protein common to all three junction types, anchoring the junctional macromolecular complexes to cytoplasmic actin. ZO-1 belongs to the family of membrane-associated guanylate kinase-like proteins (MAGUK) and incorporates three PDZ domains: an SH3 domain, a GUK domain and a proline-rich domain at the C-terminus [11]. The binding of Cx43 to the PDZ2 domain of ZO-1 regulates the size and stability of gap junction channel aggregates [12, 13]. ZO-1 governs the cellular distribution of Cx43, providing a control point for dynamic switching between gap junctional communication and non-junctional (hemichannel) communication at the perinexus – a specialized membrane domain at the periphery of gap junction channel aggregates [13, 14]. ZO-1 disruption in a functional epithelial monolayer results in a loss of barrier function and a reorganization of apical actin and myosin [15].

AMD is associated with increased VEGF secretion, which is thought to play a role in the pathologic angiogenesis accompanying the disease. However, VEGF was originally known as vascular permeability factor as it was initially observed to increase microvascular permeability and to promote accumulation of interstitial fluid [16]. Dahrouj and colleagues have convincingly shown that subretinal fluid resorption is through the RPE; a process that is impaired by VEGF [5]. VEGF is known to disrupt ZO-1 organization, resulting in tight junction disassembly and increased monolayer permeability [17, 18]. Furthermore, *in vitro* studies using endothelial cells show that VEGF-mediated disruption of gap junction communication is correlated with changes in Cx43 phosphorylation [19].

We have developed a synthetic peptide, containing a sequence that mimics the Cx43 C-terminal PDZ binding domain (17–25 amino acids), to target the interaction between Cx43 and ZO-1. αCT1 (Alpha Connexin carboxy-Terminal 1) peptide has a high binding-specificity for the PDZ-2 domain of ZO-1 and competitively inhibits interaction of proteins binding to this domain, with its binding partners, including Cx43 [12, 20, 21]. This mechanism is different from other Cx43-based peptides (Cx43 mimetics) that are thought to cause a reduction in Cx43 channel activity[22, 23] or that target the Cx43 microtubule-binding domain, which reduces hemichannel activity [24].

Treatment with the αCT1 peptide has been shown to have beneficial effects on cardiac [25–28], and cutaneous wound healing [29–33]. Importantly, topical αCT1 has been studied in four clinical trials for in indications skin wound healing with no adverse reactions, including no evidence of immune response by patients [33, 34]. Given that RPE cells are as dependent on the normal function of intercellular junctions, as are heart and skin tissues, we sought to test the effects of the peptide on ocular pathology involving the RPE. We hypothesized that stabilizing RPE cell junctions by treating with αCT1 would reduce VEGF-dependent pathology. We tested this hypothesis in two different mouse models: the laser-induced CNV model that results in angiogenesis, as well as the Light-Damage Model which shows loss of RPE cell integrity. Primary mouse RPE cells, ARPE-19 cells and MDCK cells were employed in the *in vitro* studies of the mode-of-action of αCT1.

RESULTS

Detection of αCT1 in RPE Cells

αCT1 peptide was applied via corneal eye drop application (5 mM). To confirm that αCT1 reached its target via this route, we stained for Cx43 in murine flatmount preparations. Given that the αCT1 is a peptide mimetic of the C-terminus of Cx43, we could compare the difference in the Cx43 staining pattern between animals that were treated with either αCT1 or vehicle. As expected, vehicle control animals showed Cx43 staining mostly in clusters along the lateral borders of RPE cells, representing Cx43 in gap junctions (Fig. 1B). In comparison, flatmounts from animals that were given αCT1 eye drops showed significantly more Cx43 staining both in gap junctions, as well as in the cytoplasmic compartment corresponding to free Cx43 CT ligand in the form of αCT1 (Fig. 1D). No staining was detected in no-primary-antibody controls (Fig. 1A), and αCT1-dependent staining could be eliminated by primary antibody preabsorption with excess peptide (10×) (Fig. 1C). These data were consistent with αCT1 applied to the cornea reaching the intended target tissue in quantities detectable by immunohistochemistry.

αCT1 Peptide Decreases CNV Development and Loss of Visual Function

CNV is known to be associated with an increase in the angiogenic factor VEGF in both mouse and human RPE [35], and CNV is associated with both blood vessel growth and fluid leakage induced by VEGF [36]. In order to investigate the effects of the αCT1 peptide on CNV development in 3- to 4-month-old C57BL/6J mice, CNV lesions were induced by laser photocoagulation of Bruch's membrane (BrM). Area measurements of CNV lesion size (*en face* images) (Fig. 2A–C) and area of fluid leakage (vertical section) (Fig. 2D–F) were analyzed by spectral domain-optical coherence tomography (SD-OCT). SD-OCT has been shown to allow for quantification of lesion size that correlated with *ex vivo* histological findings [37]. Here, we confirmed the development of new blood vessels (angiogenesis) by immunohistochemistry with FITC-labeled isolectin B4 (Fig. 2G, H) [38]. The peptide was administered via eye drops (5 mM of αCT1; 10 μL per eye) and its efficacy was compared to vehicle drops in four different treatment regimes. All animals were exposed to equal drug treatment, though timing was varied in order to determine the optimal treatment window for the drug. Treatment was either provided continuously (mice were treated once [in the pm] for six days on days 1–6 or 4–9) (Fig.2J, L); during the early phase of the model (animals were treated twice daily [in the am and pm] for three days on days 1–3) (Fig. 2I); or during the growth phase of the lesion (animals were treated twice daily [in the am and pm] for three days on days 4–6) (Fig. 2K). αCT1 was found to significantly reduce the growth of the CNV lesion by around 25% ($P < 0.05$) in both the 6-day continuous (Fig. 2J), as well as the 3-day early administration group (Fig. 2I). However, no significance could be established for the group that received treatment for 3-days late in the development of CNV (Fig. 2K), or those that received the delayed 6-day continuous treatment (Fig. 2L). Importantly, αCT1 was found to not only reduce the size of the fibrovascular scar (Fig. 2I–L **left-hand column**), but also to significantly reduce fluid leakage into the subretinal space (Fig. 2I–L **right-hand column**) by around 50% ($P < 0.05$) in both the early 6-day continuous, as well as the 3-day early administration groups. As seen for growth assessments, no significance could be established regarding fluid leakage for the groups receiving αCT1 treatment for 3 days in

late CNV or those receiving the delayed 6-day treatment. Finally, isolectin B4 staining of RPE-choroid flatmounts confirmed that αCT1 treatment for 3 days in early CNV reduced new blood vessel formation (Fig. 2G, H). Eyedrop application of αCT1 significantly reduced CNV volume compared with PBS (relative size in percent: PBS 100 ±7.0 versus αCT1 70 ±9.2; $P < 0.05$) with the magnitude (30%) being comparable to that obtained by OCT measurements. These data together suggest that the αCT1 peptide is required during the early phase of CNV to exert its effect on reducing fibrosis, angiogenesis and fluid leakage.

We have shown previously that CNV size correlates with loss of retinal function as measured by Ganzfeld electroretinograms (ERGs) [35]. Retinal function was assessed by recording dark-adapted ERG amplitudes. These readings allow for the analysis of the light sensitivity of the rod photoreceptors (a-wave) and the sensitivity of the bipolar cells to the cessation of glutamate-release from stimulated photoreceptors (b-wave). Vehicle- and αCT1-treated animals (n=8 per group) were compared after completing the CNV study with the early continuous treatment regimen. ERG measurements were made for 6 different light intensities (−40, −30, −20, −10, −6 and 0 dB of attenuation) (data not shown). Using a *t*-test for comparison at individual light intensities, αCT1-treated animals had significantly higher amplitudes (~15–20%) at all intensities for both a- and b-waves, as compared to controls, which was then confirmed using a repeated measure ANOVA over the different light intensities for both a-and b-waves ($P<0.001$) (see supplementary material, Fig. S1).

αCT1 Peptide Maintains RPE Cell Integrity Around CNV Lesions

CNV has at least three components; involving breakdown of the RPE, followed by angiogenesis of the choroidal vasculature and fluid leakage from these newly formed vessels. To test whether CNV size also correlated with RPE cell integrity, a subset of mice (vehicle group and animals treated for 6 days with αCT1) were sacrificed 7 days after CNV induction and the RPE/choroid was flatmounted. The flatmounts were histologically analyzed for cell junction markers, ZO-1 (Fig. 3A, B) and Occludin (Fig. 3C, D). In all animals, ZO-1 and Occludin staining revealed a halo of unhealthy RPE cells surrounding the CNV lesion. Unhealthy was defined as cells having lost junctional markers and/or normal hexagonal shape. The diameter of this halo (peri-lesion area) was significantly reduced ($P<0.05$) by αCT1 for the two cell junction markers by ~30% (measured in microns; ZO-1: control 105 ±9.2 versus αCT1 74 ±12.5; Occludin: control 96 ±13.8 versus αCT1 68.3 ±10.7). In addition, cells stained for ZO-1 or Occludin within the peri-lesion area were analyzed for eccentricity (assessing eccentricity of an ellipse; Fig. 3E) and form factor (equals 1 for a perfectly circular object; Fig. 3F) (CellProfiler software) in 4 steps of 35 μm (bins 1–4) and compared to those obtained from healthy RPE cells. Healthy RPE cells exhibit a form factor of ~0.82 and an eccentricity value of ~0.65. RPE cells from animals treated with the αCT1 peptide could be analyzed in all four bins, and exhibited form factor and eccentricity values closer to normal in the 2nd bin (35–70 μm from the edge of the lesions), whereas those treated with vehicle were so disrupted that they could not be analyzed in the 1st bin, and were significantly worse ($P>0.05$) in the 2nd bin.

Effects of the αCT1 Peptide on RPE Cell Integrity in a Light-Damage Model

It has been shown that hyper-activation of the retina via bright-light exposure leads to photoreceptor cell death in mice due, in part, to increased VEGF-mediated RPE permeability [39]. To investigate the effects of the αCT1 peptide on RPE cell integrity, RPE damage was triggered using a light-damage model (3000 lux of white light for 3 hours) in Balb/c mice. Cell morphology was determined via ZO-1 (Fig. 4A–C) and Occludin (Fig. 4D–F) immunohistochemistry in RPE flatmounts. Cell profiler software was used to determine the tiling pattern of the RPE and its morphology for animals that were pretreated with the αCT1 peptide (5 mM) compared to vehicle prior to bright light exposure (Table 1). To determine the maximum effect of the αCT1 peptide in this model, peptide was given 3-times, three hours (−3) and one hour (−1) prior to the start of light damage, as well as 15 minutes after completion of light exposure. Light damage reduced the number of cells with ZO-1 staining (Table I, ZO-1) by ~30%, as evidenced by the significant drop in cell count (P =0.004), number of neighbors (P =0.008), and the area covered (P =0.05), when compared to no light damage. In addition, cellular morphology was altered as evidenced by significant changes in form factor (P =0.017) and eccentricity (P =0.002). αCT1 treatment significantly preserved RPE morphology (Fig. 4) and cell counts (Table 1). Similar results were obtained when analyzing Occludin distribution by immunohistochemistry and image analysis (Table 1, occludin). To determine the treatment window for αCT1 application, animals were divided into groups, administering only one dose of treatment at the following time points: −4, −2, −1, +1, +4 and +6 hours with the zero time point representing light ON. RPE flatmounts were analyzed using ZO-1 immunohistochemistry. Measurements were significant (P <0.05) for most of the morphometric measures when animals were pre-treated with αCT1 compared to vehicle, irrespective of the amount of pretreatment; yet none of the factors reached significance when treatment was delayed, post-light onset (Table 2). These results indicate that bright light triggers rapid damage in the RPE, which cannot be prevented when treatment is delayed.

Effects of the αCT1 Peptide on Reduction of Barrier Function

For mechanistic studies, we switched to assessing barrier function in ARPE-19 cells, a human RPE cell line. ARPE-19 cells were chosen since when grown as monolayers they express the signature genes of human RPE cells [40], and develop tight junctions and resemble an aged RPE [41] over time. RPE cell health and monolayer integrity was confirmed by immunohistochemistry for ZO-1, Occludin and β-actin, revealing the presence of these junctional markers at cell-borders, actin filament distribution in the form of circumferential bundles and ZO-1, actin filaments co-staining at the cell borders (Fig. 5A–D). Results in ARPE-19 cells were verified in primary mouse RPE cultures. Transepithelial resistance (TER) measurements are a standard assay of tight junction integrity [42]. VEGF has previously been shown to alter tight junction structure and promote leakage in RPE monolayers, resulting in a reduction of TER. This loss in VEGF-induced TER can be prevented by co-administration of a VEGF-R2 receptor antagonist [42]. Here, we showed that VEGF prompted a reduction in TER in a time-dependent manner in both ARPE-19 cells (Fig. 5E) as well as in primary mouse RPE cells (Fig. 5F), which was ameliorated by pre-incubating the cells with αCT1. After having confirmed the primary premise in both ARPE-19 cells as well as primary mouse RPE cells, the remainder of the pathway analysis

was performed in ARPE-19 cells. Short-term incubation with αCT1 did not alter TER significantly over the 4-hour time course of this experiment (Fig. 5E); however, growing ARPE-19 cell monolayers in the presence of αCT1 during the timeframe from confluency (day 0 in Fig. 5G) to the establishment of maximal TER (day 12 in Fig. 5G) demonstrated that αCT1 aided in the time course of the establishment of barrier function (slope; control: 4.10 ±0.40 versus αCT1: 7.29 ±0.54; P <0.001), but did not raise TER above levels reached in untreated controls.

Effects of the αCT1 Peptide *In Vitro* and *In Vivo* on Cx43 Channels

The data presented thus far demonstrates that αCT1 inhibits VEGF-induced CNV growth in vivo and VEGF-induced TER reduction in ARPE-19 cells in vitro, likely by effects on tight junctional stability. However, since there is evidence that VEGF can also transiently disrupt endothelial gap junction function [19], we sought to determine whether the mode-of-action of αCT1 on RPE integrity might also involve modulation of gap junction channel activity. To test this possibility, we added the gap junction blocker, 18 beta-glycyrrhetinic acid (GCA) (0.1 mM), to the ARPE-19 TER assay (Fig. 5H) [43]. Administration of the gap junction inhibitor alone had little effect on TER. Additionally, there was no significant difference in TER between cells that received VEGF (10 ng/mL) only and wells where VEGF and 18-beta GCA were added together. Addition of αCT1 peptide ameliorated the effects of VEGF-mediated TER reduction, with or without 18-beta GCA, suggesting that the gap junction channel blocker was not required for a TER protective effect.

A further mechanism of connexin-dependent cell communication involves extra-cellular or paracrine communication via unpaired connexon hemichannels [44]. Hemichannels allow for communication between the intracellular compartment and the extracellular environment. Signaling molecules released by hemichannels include ATP, which among its other functions serves as an autocrine signaling ligand for purinergic receptors. Extracellular ATP has been demonstrated to be important for calcium signaling activation, as well as in regulating ion and fluid transport in the RPE [44, 45]. Rhett and colleagues showed that αCT1 can recruit hemichannels into gap junctions, thereby indirectly reducing the pool of hemichannels available for signaling [13]. If VEGF-treatment prompted the release of ATP via hemichannels, then apyrase (1 U/mL), an ATP/ase and ADP/ase, should prevent VEGF-induced loss in TER [46]. However, apyrase, without or without VEGF, significantly (P <0.05) reduced TER (Fig. 5I), suggesting that reduction in extracellular ATP, whether resulting from Cx43 hemichannel inhibition or another mechanism, was unlikely to account for αCT1-mediated maintenance of TER.

To directly test whether or not hemichannels are involved in VEGF-induced loss of TER by ARPE-19 cells, we used a novel selective blocker of these channels - JM2 [24]. As with apyrase, JM2 was found not to affect the VEGF-induced loss in TER, but significantly (P <0.002) reduced resistance when applied alone (Fig. 5J). This led us to conclude that inhibition of hemichannel function in ARPE-19 cells resulted in destabilization of barrier function. Indeed, we observed that hemichannel downregulation had the opposite effect of what might be expected if increased activity of hemichannels accounted for TER loss by ARPE-19 cells.

Based on the results from ARPE-19 cultures, we surmised that JM2-mediated inhibition of Cx43 hemichannels in our mouse CNV model should result in increased injury spread. Consistent with its observed effect on ARPE-19 barrier function, JM2 increased, rather than decreased, the size of the fibrovascular scar (Fig. 2C, M). There was also a significant (P <0.05) increase in fluid leakage into the subretinal space (Fig. 2F, M) (control 13% vs JM2 21%) as assessed by spectral domain-optical coherence tomography. Taken together, the data gathered both in vivo and in vitro indicated that connexin hemichannels were not likely mechanistically involved in stabilization of barrier function by αCT1.

Effects of the αCT1 Peptide on Tight Junction-mediated TER independent of Cx43

Cx43 is well characterized as having both channel and non-channel dependent functions [47, 48]. In the previous section we provided evidence that the effects of aCT1 on TER were unlikely to occur via Cx43 channel activity of any type. Nonetheless, RPE cells in vivo and in primary culture in vitro express readily detectable levels of Cx43 [49, 50]. ARPE-19 cells also express a notably elevated level of Cx43. To exclude any potential effect of Cx43 (channel independent or otherwise), we tested αCT1 effects on barrier function in MDCK cells (Fig. 6), which not only are a well-studied model of tight junction dynamics [51], but express no to almost non-detectable amounts of Cx43 [52]. Barrier function was tested using two different techniques, transepithelial resistance measurements (Fig. 6A) and electric cell-substrate impedance sensing (ECIS) assays (Fig. 6B) before and after EGTA (ethylene glycol tetraacetic acid) treatment, a trigger that disassembles tight junctions in MDCK monolayers [51]. Acute EGTA treatment (1.2 mM) significantly decreased barrier function as measured by TER (P <0.01 vs. corresponding control). EGTA triggered a larger percentage decrease in PBS- (73.6 ± 4.7%; n=6), as compared to αCT1-pre-treated cells (28.0 ± 7.7%; n=6; P <0.01 vs. untreated cells). In analogy to the experiments, in which it was shown that αCT1 accelerated the time course of the establishment of barrier function (Fig. 5G), re-establishment of barrier function after calcium chelation was examined in MDCK monolayers. After EGTA treatment (0.5 mM), which decreased barrier function as measured by ECIS, physiological levels of calcium were restored by providing fresh medium containing 1.8 mM $CaCl_2$. Recovery of barrier function was significantly slower in PBS-, as compared to αCT1-treated cells (P <0.05).

Taken together, αCT1 stabilized tight junctions in two independent models (ARPE-19 and MDCK cell monolayers) triggered by two methods (VEGF and calcium-chelation), in a manner that appears to be independent of Cx43 function.

DISCUSSION

αCT1 is a clinically tested, peptide-based therapeutic that competitively blocks interactions at the PDZ2 domain of ZO-1, thereby inhibiting ligands that selectively bind to this domain. Here, we analyzed the effects of αCT1 in *in vivo* and *in vitro* models of VEGF-dependent RPE damage. The main results of the *in vivo* components of this study were as follows: (a) αCT1 delivered topically via eye drops accumulated in the RPE where it could be detected by immunohistochemistry; (b) αCT1 significantly reduced laser-induced CNV when applied during the initiation or trigger phase of CNV development, rather than during the growth

phase; and (c) αCT1 significantly improved RPE morphology *in vivo* after bright-light exposure, a stimulus that alters RPE morphology in a VEGF-dependent manner. The *in vitro* RPE assays, together with the *in vivo* CNV mouse experiments, suggested a mode-of-action that was separate from both Cx43 channel and non-channel dependent functions and involved αCT1 prevention of VEGF-induced loss of transepithelial resistance, CNV growth and RPE-cell damage via the stabilization of tight junctions. Taken together, our data indicate that αCT1-mediated stabilization of tight junctions may serve as a new treatment paradigm for both wet and dry AMD.

The RPE is a barrier epithelium located between the retina and the choroid. This outer blood retina barrier is essential to proper function of the eye, as the epithelial barrier supports nutrient and solute transport, while preventing infiltration of cells (choroidal epithelial cells or inflammatory cells) into the subretinal space. As such, the RPE is involved in maintaining fluid balance within the retina and removing excess interstitial fluid [5]. Together with its basement membrane, BrM, and the RPE cell plasma membranes, the primary cellular determinants of the RPE barrier function are tight junctions between RPE cells in the monolayer. RPE cell damage and concomitant loss of outer blood retina barrier are common features in dry and wet AMD, as well as in the formation of macular edema, which contributes to pathology in diabetic retinopathy. Outer blood retina barrier loss involves inflammation, angiogenesis, and oxidative stress; and VEGF and other growth factors are involved in mediating this loss of barrier function in the RPE, as well as angiogenesis and choroidal neovascularization.

We have identified and developed a novel peptide, αCT1. αCT1 is a soluble 25 amino acid peptide (3597.33 MW) that has a compact 2-domain design based on linkage of an antennapedia (a cellular membrane transport peptide) internalization domain (1–16 amino acids; RQPKIWFPNRRKPWKK) to the C-terminal PDZ binding domain of Cx43 (17–25 amino acids; RPRPDDLEI). This Cx43 mimetic binds to its respective binding partners, including the PDZ2 domain of ZO-1, an essential component of tight junctions, thereby interfering with the target protein's normal function(s).

In the current study, we were able to show translocation of the αCT1 peptide to the RPE following topical corneal application. Compounds applied to the cornea are expected to reach the posterior pole via the trans-scleral route [53] and biodistribution is affected by potential binding to melanin, present in the RPE/choroid [54]. In ongoing work, we are planning to comprehensively address the bioavailability of aCT1 administered via this ocular route.

To determine the therapeutic possibility of targeting tight junctions with αCT1 in the treatment of ocular pathology, we chose two animal models that exhibit VEGF-dependent RPE pathology: a mouse model of choroidal neovascularization (CNV), and a model of light-induced RPE damage in Balb/c mice. In both models, anti-VEGF blocking strategies have been shown to prevent or reduce pathology [39, 55]. Here, we demonstrated that the αCT1 peptide significantly reduced CNV development when treatment was initiated at the time of laser photocoagulation. The reduction of CNV development correlated with healthier RPE cells found closer to the lesion site (peri-lesion area) in the αCT1-treated group

compared to controls. A reduction in CNV development also correlated with improved retinal function, as shown in the higher rod ERG a-and b-wave amplitudes elicited by mice treated with the peptide. αCT1 also improved cell morphology in the light-damage model of RPE barrier function loss. Similar to what was found with CNV, αCT1 significantly reduced RPE damage when treatment was initiated prior to the onset of toxic levels of light exposure. Taken together, these data indicate that αCT1 peptide preserves RPE structure and presumably barrier function in these models of VEGF-induced ocular pathology.

Our present understanding of the mechanism of αCT1 is based on its demonstrated ability to modulate the interaction between Cx43 and its C-terminal binding partners, including ZO-1 [12, 13]. ZO-1 is a critical tight junction protein and regulates the cellular distribution of Cx43, providing a control point for dynamic switching between gap junction communication and non-junctional hemichannel communication [13, 14]. In order to determine a potential mechanism in ameliorating disease of the RPE, we examined the effects of αCT1 on tight junction integrity, in connection with Cx43-mediated gap- and hemichannel communication. TER assays provide a simple measure of paracellular barrier integrity [42]; and TER deteriorates in response to VEGF-mediated disassembly of tight junctions. TER assays on ARPE-19 cells were conducted to determine whether αCT1 would prevent VEGF-mediated TER breakdown. VEGF is known to induce tight junction permeability by trafficking Occludin fragments away from the tight junction site, as well as by Occludin and ZO-1 phosphorylation [18, 56, 57]. In addition, VEGF transiently disrupts gap junction communication in endothelial cells [19]. We found that 100 μM of αCT1, a concentration shown to be biologically active in HeLa cells [12], prevented the loss of barrier function in RPE cells that is induced by 10 ng VEGF. However, ARPE-19 cells express, some but not all tight junction proteins, notably ZO-1 and Occludin, but apparently do not express claudin (human RPE cells predominantly express claudin-19), and exhibit lower TER development than their *in vivo* counterparts [58]. We therefore confirmed the effects of αCT1 on barrier function in two ways, in primary mouse RPE cells, as well an independent model, calcium-chelation-induced tight junction disassembly in MDCK cells. Mouse RPE cells have been shown to express claudins 1 and 3 [59] and develop TER in culture [60]. And the results on MDCK cells not only provided an additional independent and well-studied model to examine tight junction dynamics [40], but more importantly, these cells express almost non-detectable levels of Cx43 [41]. As such, αCT1 effects on tight junction integrity and barrier function in this model likely occurred independent of its effects on Cx43 activity.

Further evidence that αCT1 mediated effects were not dependent on Cx43 function in the models of RPE pathology came from experiments in which gap junction channel function was targeted directly. Blocking intercellular communication via the gap junction inhibitor, 18-beta GCA, had little effect on barrier function in TER assays, and 18-beta GCA did not modify the response to VEGF. However, αCT1 still inhibited TER loss when VEGF and 18-beta GCA were coadministered- suggesting that gap junctions were not involved in the effects of αCT1 on barrier function. Another mechanism by which αCT1 could stabilize RPE barrier function is via Cx43 hemichannel activity. ATP is one of the most abundant extracellular signaling molecules and plays a pivotal role in intercellular communication via autocrine and paracrine signaling, and its release, in part, is mediated by hemichannels [46]. ATP has been shown to both increase and decrease endothelial barrier function, based on

whether the response is mediated by ATP or its metabolite, adenosine [61]. Furthermore, there is evidence that the release of ATP can promote wound healing in epithelial cells [62]. The latter might be the reason why disrupting ATP communication via the ATP diphosphohydrolase apyrase or by reducing hemichannel activity using JM2, resulted in a significant decrease in TER when added to monolayers. If the VEGF effects on TER did involve Cx43 hemichannel-mediated ATP release, co-administering VEGF and apyrase or VEGF and JM2 should have altered the degree of change produced by VEGF alone. However, adding apyrase, together with VEGF, or JM2 with VEGF showed no greater TER reduction than adding VEGF alone. Furthermore, addition of αCT1 in these assays showed no additional protective effect, again suggesting that Cx43 channel activity was not likely involved in the paradigm understudy here.

Finally, αCT1 when applied during the maturation phase of the RPE monolayer, or during the recovery phase after calcium chelation in the MDCK monolayer, the peptide accelerated barrier formation, a response known to be accounted for by time-dependent increases in tight junction assembly and stability [63, 64]. And importantly, *in vivo* treatment of CNV animals with JM2 eyedrops, significantly increased CNV area, as well as the area of fluid accumulation, as compared to PBS controls. Together, these data suggest αCT1 stabilizes barrier function by preventing the disassembly of tight junctions by a mechanism that is independent of gap-junction channel or hemichannel function [12]. While we have only tested the effects of αCT1 on barrier function in epithelial cells (RPE and kidney), we expect similar effects on endothelial cells of the choroid, contributing to the reduction in fluid leakage from newly formed vessels in CNV.

It is predicted that αCT1 has direct effects on tight junction stability based on its design as a Cx43 mimetic. The C-terminus of Cx43 and related connexins are the only proteinaceous PDZ-binding ligands known to interact with the ZO-1 PDZ2 domain. For example, a phage display-based search for PDZ2 ligands was unable to identify further interacting peptides [65]. However, the PDZ2 domain does mediate homomeric interactions with other PDZ2 domains, enabling the formation of domain-swapped ZO-1 homodimers [66]. ZO-1 dimerization promotes claudin polymerization, and increases tight junction formation and stability *in vivo* [66–68]. Domain-swapped PDZ2 dimerization also promotes high affinity binding of the Cx43 C-terminus to ZO-1 [69]. Endogenous Cx43 C-termini are not thought to interact directly with the macromolecular complexes forming tight junctions. However, the presence of free Cx43 C-termini in the form αCT1 could provide for ligand-based stabilization of ZO-1 homodimers – via αCT1 interaction within the binding pocket generated by PDZ2-PDZ2 dimeric interaction. In future work, it will be interesting to test the hypothesis that αCT1 stabilizes tight junctions by enhancing the stability of the ZO-1-containing quaternary complexes known to enhance tight junction formation and maintenance.

An additional potential mechanism that warrants investigation is based on observations that at the tissue level, αCT1 treatment is associated with reduction in pro-inflammatory cytokines and decreased inflammatory responses [70–72]. In AMD, this mode-of-action may mediate responses elicited from RPE cells, or inflammatory cells such as Mueller cells, astrocytes and glial cells as well as invading leukocytes, all of which express Cx43.

Inflammation has been shown to contribute to CNV lesion size and fluid leakage in AMD [73]. Likewise, a chemokine-mediated inflammatory response has been shown after light-damage, involving RPE cells, Mueller cells and activated microglia [74]. In addition, it has been reported that Cx43 expression in the choroid co-localizes with markers of oxidative stress and inflammation [75]. And finally, the effects on tight junction stability may occur indirectly, by the well-characterized anti-inflammatory effect of αCT1 (inflammation causes tight junction disassembly) [76–78], These additional mechanisms will be investigated in future studies; although the dynamic range of the animal models may not allow for an assignment of relative contributions between the different mechanisms.

The most widely used treatment for wet AMD is administration of anti-VEGF antibodies - intraocular injection of this treatment being necessary owing to the inability of antibodies to penetrate the immune-privileged interior of the eyeball. This treatment has improved the standard of care for AMD, however, it widely recognized that anti-VEGF is far from ideal. Altered VEGF homeostasis and/or anti-VEGF treatment have been linked to RPE pathology and geotrophic atrophy (GA) of the retina. One recent study reported a decrease in plasma levels of PEDF, the main antiangiogenic factor, in patients with dry AMD [79]; and importantly, conversion of wet to dry AMD in patients receiving anti-VEGF therapy is seen frequently [80].

RPE cells have been shown to take up anti-VEGF drugs, affecting VEGF metabolism both intra-and extracellulary [81], and in mice, ablation of VEGF in RPE cells only, was found to lead to vision loss and ablation of the choriocapillaris [82]; together reinforcing the importance of VEGF for normal ocular health and function. Hence, it is paramount to develop alternate strategies that provide a therapeutic balance between drying out wet AMD and stabilizing the RPE.

Here, we show that αCT1 peptide can be administered as topical eyedrops, without the need for intraocular injection, and that this treatment reduced VEGF-induced pathology in two *in vivo* mouse models, with effects including fibrosis and angiogenesis reduction, as well as decreasing sub-retinal fluid accumulation and loss of RPE structure. Targeting tight junction stability via topical αCT1 may serve as a promising new treatment paradigm for both wet and dry AMD, as well as other retinal diseases in which the RPE barrier is affected, either as monotherapy, or in combination with existing therapeutics.

METHODS

Animals

Albino Balb/c mice were generated from breeding pairs obtained from Harlan Laboratories to be able to maintain control over light-exposure history. Pigmented C57BL/6J mice were based on Jackson Laboratory breeding colonies. The animals were housed in the Medical University of South Carolina animal care facility under a 12-hour light / 12-hour dark cycle with access to food and water *ad libitum*. All experiments were conducted in accordance with the ARVO Statement for the Use of Animals in Ophthalmic and Vision Research and were approved by the Medical University of South Carolina Institutional Animal Care and Use Committee.

αCT1 Peptide Treatment

For *in vivo* studies, the αCT1 peptide (FirstString Research, Inc., Mount Pleasant, SC) or the JM2 peptide (amino acids 231–245 [VFFKGVKDRVKGRSD]; synthesized at American Peptide Company; Sunnyvale, CA) [24] was administered via eye drops (5 mM; 10 μL per eye) formulated in a 0.05% Brij-78 and 0.9% NaCl solution. The control group received the vehicle solution. The treatment schedule varied for individual experiments. Cell culture experiments were performed with 30–100 μM αCT1, diluted in sterile water. A one-hour pre-incubation period of αCT1 was employed for all *in vitro* experiments.

Laser-Induced CNV and Treatment Schedule

To induce CNV lesions, 3- to 4-month-old C57BL/6J mice were anesthetized (xylazine and ketamine, 20 and 80 mg/kg, respectively) as previously described [35]. Mouse pupils were dilated using 2.5% phenylephrine HCL and 1% atropine sulfate. In order to avoid cataract formation, mice were treated with Goniovisc (HUB Pharmaceuticals, Rancho Cucamonga, CA) before and after laser treatment. Laser photocoagulation was induced via a 532 nm Argon laser (100 μM spot size, 0.1 s duration, 100 mW), in which 4 equidistant laser lesions were produced surrounding the optic nerve. The formation of a bubble at the site of photocoagulation indicated the desired rupture of the Bruch's membrane [83].

Three αCT1 peptide treatment regimens were employed for CNV studies in order to establish the treatment window of the drug. For the early administration model, mice were treated twice each day (am and pm) for the first three days post laser photocoagulation. In the continuous treatment paradigm, the animals were only given eye drops once each day for 6 days. For the late administration model, the effects of the αCT1 peptide were investigated when treating the animals twice daily (am and pm) during the last three days of the CNV study. Finally, the continuous treatment paradigm was repeated with the animals receiving eye drops once each day for 6 days starting on day 4 to determine whether progression could be slowed as shown previously with a different inhibitor [38]. Thus, all four treatment regimens resulted in equal drug exposure. As a control, a connexin43 peptide known to target hemi-channel formation rather than tight junction stabilization (JM2) was applied using the early administration paradigm. Animals were euthanized after the OCT analysis in order to obtain RPE/choroid samples for the immunofluorescence studies (see Immunofluorescence Staining).

Assessment of CNV Lesions by OCT and Immunohistochemistry

CNV size was determined using optical coherent tomography (OCT) [84]. OCT was performed using an SD-OCT system (Bioptigen Inc., Durham, NC), with scan parameters set to 1.6 × 1.6 mm rectangular volume scans, consisting of 100 B-scans (1000 A-scans per B scan). Mice were anesthetized and pupils were dilated as described above. Using the Bioptigen SD-OCT system, the center of the lesion was determined by identifying the midline of the RPE/Bruch's membrane rupture [84], and Image J software (http://imagej.nih.gov/ij/) was used to measure the cross-sectional area of the hyporeflective spot seen in the fundus image (*en face*) as well as the area of fluid accumulation in the outer retina (cross-sectional view).

Assessment of CNV Lesions by Immunohistochemistry

Angiogenesis was determined in flat-mount preparations of RPE-choroid stained with isolectin B, which binds to terminal β-D-galactose residues on endothelial cells and selectively labels the murine vasculature) [85]. Immunohistochemistry, confocal microscopy and volume measurements were performed as described previously [38]. In short, eyes were collected and immersion-fixed in 4% paraformaldehyde and eyecups prepared. Standard immunohistochemistry was performed, using FITC-labeled Isolectin B (1:100 of 1 mg/mL solution; Sigma-Aldrich, St. Louis, MO). Flattened eyecups were coverslipped (Fluoromount; Southern Biotechnology Associates, Inc., Birmingham, AL), and examined by confocal microscopy (Leica TCS SP2 AOBS, Leica Bannockburn, IL). Z-stacks of images at 2 μm steps were collected through the entire depth of the CNV lesion at a single laser intensity setting for all experiments. For each slice through a lesion (i.e., region of interest) the overall fluorescence was determined to obtain pixel intensity against depth, from which the area under the curve. Individual CNV lesions were also photographed using a microscope (Zeiss, Thornwood, New York) equipped for fluorescence and digital microscopy (Spot camera; Diagnostic Instruments, Sterling Heights, MI).

Electroretinography

Electroretinography (ERG) recordings were performed as previously described [86, 87]. In short, C57BL/6J mice were dark-adapted overnight and anesthetized with xylazine and ketamine (20 and 80 mg/kg, respectively). Pupils were dilated with phenylephrine HCL (2.5%) and atropine (1%). ERGs were recorded with the UTAS-2000 (LKC Technologies, Inc., Gaithersburg, MD) system, using a Grass strobe-flash stimulus. Stimuli consisted of 10 μs single-flashes at a fixed intensity (2.48 $cd*s/m^2$) under scotopic conditions. ERG measurements were performed before (baseline ERG) laser photocoagulation, and afterwards on day 6. A-wave amplitudes were measured from baseline to the a-wave trough, whereas b-wave amplitudes were measured from the a-wave trough to the peak of the b-wave.

Bright Light Exposure Protocol and Treatment Schedule

Six-week-old Balb/c mice were exposed to bright light for 3 hours using 3000 lux after 12 hours of dark adaptation [88]. The light exposure box was wrapped in aluminum foil to increase reflectivity. Mouse pupils were dilated using 2.5% phenylephrine HCL and 1% atropine sulfate 15 minutes prior to the exposure of bright light.

Different treatment groups were established. To establish proof of principle, animals received αCT1 eye drops (5 mM, see αCT1 Peptide Treatment) three hours and one hour prior to the start of light damage, as well as 15 minutes after completion of light exposure. The control group was given vehicle drops at the same time points. For comparison, one group of animals did not receive any bright-light exposure. To establish the therapeutic window for αCT1, 6 additional groups of mice were treated 4, 2, and 1 hour prior to bright-light exposure, as well as 1, 4 and 6 hours post bright-light exposure. All animals were euthanized 24 hours post light damage in order to collect RPE/choroid flatmounts. RPE cells were stained (see Immunofluorescence Staining) with ZO-1 and occludin for morphometric analysis via the cell profiler software (cellprofiler.com).

Immunofluorescence Staining

Eyes were collected and lens, anterior chamber, and retinas were removed rapidly [35]. Eyecups were immersion-fixed in 4% paraformaldehyde (PFA) overnight at 4°C. After extensive washing, eyecups were either incubated in antibodies recognizing ZO-1 (1:200; Cat# 61–7300, Invitrogen, Carlsbad, CA), occludin (1:200; Cat# 71–1500, Invitrogen) or connexin43 (1:300; Cat# C6219, Sigma Aldrich, St. Louis, MO) in blocking solution (10% normal goat serum, and 0.4% Triton-X in tris-buffered saline). All the before-mentioned antibodies are rabbit polyclonal; thus, Alexa Fluor 488 goat-anti-rabbit (1:500; Cat# A-11008, Invitrogen) was used as the secondary antibody. Following extensive washing, eyecups were flattened using four relaxing cuts and cover-slipped using Fluoromount (Southern Biotechnology Associates, Inc., Birmingham, AL). For some experiments, connexin43 antibody was preabsorbed with 10× molar excess of αCT1 peptide. Staining was also performed on ARPE-19 cells that were grown on Transwell® filters (3450, Costar; Sigma Aldrich). All immunohistochemistry experiments included a no-primary antibody control. To analyze the monolayers, cells were fixed in 4% PFA at room temperature for 10 minutes. The same protocol and agents were employed for the cells as described for the *ex vivo* studies. In addition, cells were stained with Alexa Flour 647 phalloidin according to the manufacture's recommendations (Cat# 8940S, Cell Signaling Technology, Danvers, MA). Staining of cells and flatmounts was examined via fluorescence microscopy (Zeiss, Thornwood, NY) equipped with a digital black-and-white camera (Spot camera; Diagnostic Instruments, Sterling Heights, MI).

Assessment of RPE morphology

Images of flatmounts were imported as TIF files into CellProfiler v2.1.1 for analysis (http://www.cellprofiler.org/). For each comparison, images of equal size and exposure time were analyzed, using a customizable script. The pipeline "neighboring cells" was used. For each image, we obtained cell count (number of cells present), form factor (equals 1 for a perfectly circular object), eccentricity (measures the degree to which an object represents an ellipse, and varies between 0 and 1), number of neighbors (a perfect hexagonal RPE cell has 6 neighbors), perimeter (the total length of the perimeter of all the RPE cells present in the image), and the total area covered by the RPE cells (determines the degree of loss of cells). The tiling patterns of RPE cells in the peri-lesion area surrounding the CNV lesions were analyzed in 35×75 μm (depth by width) bins. Results were exported into Excel for statistical analysis.

Cell Cultures

ARPE-19 cells, a human RPE cell line, was expanded in Dulbecco's modified Eagle's medium (DMEM) (Invitrogen) with 10% fetal bovine serum and antibiotics as previously described [89]. These cells generate a polarized RPE cell monolayer when plated on Transwell® filters based on the following criteria: polarized secretion of VEGF [90], polarized expression of VEGF-R2 receptors (35) and hence polarized susceptibility to compounds that trigger VEGF-secretion [42, 90], polarized expression of complement inhibitors [90], and the presence of circumferential actin bundles (see Fig. 5A).

Primary mouse RPE cells were prepared following our published protocol [60] with modifications [91]. Pups (10 days old) were sacrificed by decapitation. Eyes were removed, washed in HBSS without Ca^{+2} or Mg^{+2} with 10 mM HEPES and placed in growth medium (GM) containing MEM-A supplemented with 1× Glutamax, 1× penicillin/streptomycin, 1× MEM nonessential amino acids, 20 μg/l hydrocortisone, 250 mg/l taurine, 0.013 μg/L triiodo-thyronin + 10% FBS. Eyes (batches of 10) were incubated in 5 mL of dispase II (45 min at 37°C), followed by quenching in GM. Posterior eyecups were dissected and incubated in GM for 20 min at 37°C, which facilitates the removal of the neural retina. Intact sheets of RPE were then peeled-off, washed with GM (3×) followed by Ca^{2+}- and Mg^{2+}-free Hanks' balanced salt solution. RPE sheets were triturated using a serological pipette, and cells sedimented by centrifugation (2 min at 300*g*). The cells were resuspended in 1 mL 0.05% trypsin EDTA to break down remaining clumps of tissue (37°C for 1 min), followed by enzyme quenching in GM and sedimentation. The cells were resuspended in 4.5 mL GM and 0.5 mL was plated on each transwell (12-well) for final experiments (equivalent to ~2 eyes per well).

MDCK cells were obtained from ATCC (American Type Culture Collection, Manassas, VA) and grown on permeable Transwell® filters in DMEM supplemented with 10% FBS, and 1% PenStrep (5000 U/mL). MDCK cells are a well-studied model of tight and adherence junction dynamics [51], in which surface polarity develops concomitantly with the development of TER [64].

For TER measurements, ARPE-19, primary RPE cells or MDCK cells were grown on permeable membrane inserts in the presence of media with 10% fetal bovine serum and antibiotics. After cells became confluent, serum was reduced to 2% and monolayers were grown for another ~2–3 weeks. Cells were exposed to serum-free media the last two days prior to the measurements. Barrier function requires a stable TER, where high TER is indicative of the robust RPE [42] or MDCK [64] barrier properties afforded by tight junctions. TER was monitored with an epithelial volt-ohm meter (World Precision Instruments, Sarasota, FL) equipped with an STX2 electrode. Measurements using this electrode are very reliable, with percent errors of <5% between repeat measures. Maximal TER values are reached within 2–3 weeks after cells reach confluency. The TER value for cell monolayers was determined by subtracting the TER for filters without cells. Agents used for the TER assays were VEGF165 (Cat# SRP4363; Sigma Aldrich), EGTA, 18-beta glycyrrhetinic acid (Cat# G10105, Sigma Aldrich), apyrase (Cat# M0398S; New England Biolabs, Ispwich, MA), αCT1, and the connexin 43 hemichannel blocker, JM2 [24].

For impedance measurements, 10^5 MDCK cells were plated into each well of an 8-well 10E + ECIS (Electric Cell-substrate Impedance Sensing) dish, and impedance measured over frequencies ranging from 62.5 Hz to 64 kHz every 80 seconds using the ECIS system (Ididi; Madison WI). Barrier function was quantified as the real component of the impedance at frequencies below 2.5 kHz [92, 93]. In short, cells were allowed to proliferate overnight before treatment with 0.5 mM EGTA. Calcium chelation by addition of EGTA is an accepted model to study the dynamics of tight junctions and has been shown to reliably induce their disassembly [51]. After 40 minutes, physiological levels of calcium were restored by providing fresh medium containing 1.8 mM $CaCl_2$, and recovery of impedance was

investigated in the presence of 100 μM αCT1 or vehicle (PBS) by continued ECIS measurements. The ratio of barrier function following αCT1 treatment to the minimum barrier function in response to EGTA treatment was calculated as an index of the effects of αCT1.

Statistical Analysis

Data are presented as mean ± SEM or mean ± SD as indicated. Single comparisons were analyzed by *t*-test analysis, accepting a significance level of $P<0.05$. Repeated ANOVA measurements were conducted for ERG and time-course TER studies.

Supplementary Material

Refer to Web version on PubMed Central for supplementary material.

Acknowledgments

Funding for this project was provided in part by the Feldberg Endowment (BR), the National Institutes of Health (NIH) (R01 EY019320 to BR and R01 HL56728 to RGG), Department of Veterans Affairs (I01 RX000444), Foundation Fighting Blindness, an unrestricted grant to MUSC from Research to Prevent Blindness (RPB), Inc., New York, NY, as well as FirstString Research, Inc. (firststringresearch.com) (GSG, President and CEO; and CG, Director of Translational Research, both in advisory roles) through NSF grant IIP-1215149. No employees of FirstString Research were directly involved in study data collection; decision to publish and the writing of the manuscript (EO and BR). Animal studies were conducted in a facility constructed with support from the NIH (C06 RR015455).

Funding for this project was partially provided by FirstString Research Inc., as a means of investigating translational research models for the αCT1 peptide and to determine the peptide's method of action. FirstString Research holds the exclusive patent for αCT1 (US 7786074; US 7888319B2; US 8357668; US20110130345 A1). BR and RG are inventors of the patent for composition and methods for use in treating or preventing macular degeneration (US20110130345 A1).

REFERENCES

1. Brown MM, Brown GC, Stein JD, Roth Z, Campanella J, Beauchamp GR. Age-related macular degeneration: economic burden and value-based medicine analysis. Canadian Journal of Opthalmology. 2005; 40:277–287.
2. Tomany SC, Wang JJ, Van Leeuwen R, Klein R, Mitchell P, Vingerling JR, Klein BE, Smith W, De Jong PT. Risk factors for incident age-related macular degeneration: pooled findings from 3 continents. Ophthalmology. 2004; 111:1280–1287. [PubMed: 15234127]
3. Hageman, Gregory S., Luthertb, Phil J., Victor Chong, NH., Johnsonc, Lincoln V., Don Andersonc, H., Mullinsa, RF. An Integrated Hypothesis That Considers Drusen as Biomarkers of Immune-Mediated Processes at the RPE-Bruch's Membrane Interface in Aging and Age-Related Macular Degeneration. Progress in Retinal and Eye Research. 2001; 20:705–732. [PubMed: 11587915]
4. Strauss O. The Retinal Pigment Epithelium in Visual Function. Physiological Reviews. 2005; 85:845–881. [PubMed: 15987797]
5. Dahrouj M, Alsarraf O, McMillin JC, Liu Y, Crosson CE, Ablonczy Z. Vascular endothelial growth factor modulates the function of the retinal pigment epithelium in vivo. Invest Ophthalmol Vis Sci. 2014; 55:2269–2275. [PubMed: 24550368]
6. Peng S, Gan G, Rao VS, Adelman RA, Rizzolo LJ. Effects of proinflammatory cytokines on the claudin-19 rich tight junctions of human retinal pigment epithelium. Invest Ophthalmol Vis Sci. 2012; 53:5016–5028. [PubMed: 22761260]
7. Sohl G, Willecke K. Gap junctions and the connexin protein family. Cardiovasc Res. 2004; 62:228–232. [PubMed: 15094343]

8. Hoang, Quan V., Haohua, Qian, Ripps, H. Functional analysis of hemichannels and gap-junctional channels formed by connexins 43 and 46. Molecular Vision. 2010; 16:1343–1352. [PubMed: 20664797]

9. Gonzalez-Mariscal L, Betanzos A, Nava P, Jaramillo BE. Tight junction proteins. Prog Biophys Mol Biol. 2003; 81:1–44. [PubMed: 12475568]

10. Meng W, Takeichi M. Adherens junction: molecular architecture and regulation. Cold Spring Harbor perspectives in biology. 2009; 1:a002899. [PubMed: 20457565]

11. Bauer H, Zweimueller-Mayer J, Steinbacher P, Lametschwandtner A, Bauer HC. The Dual Role of Zonula Occludens (ZO) Proteins. Journal of Biomedicine and Biotechnology. 2010; 2010:1–12.

12. Hunter AW, Barker RJ, Zhu C, Gourdie RG. Zonula occludens-1 alters connexin43 gap junction size and organization by influencing channel accretion. Mol Biol Cell. 2005; 16:5686–5698. [PubMed: 16195341]

13. Rhett JM, Jourdan J, Gourdie RG. Connexin 43 connexon to gap junction transition is regulated by zonula occludens-1. Mol Biol Cell. 2011; 22:1516–1528. [PubMed: 21411628]

14. Martin P, Parkhurst SM. Parallels between tissue repair and embryo morphogenesis. Development. 2004; 131:3021–3034. [PubMed: 15197160]

15. Van Itallie CM, Fanning AS, Bridges A, Anderson JM. ZO-1 Stabilizes the Tight Junction Solute Barrier through Coupling to the Perijunctional Cytoskeleton. Molecular Biology of the Cell. 2009; 20:3930–3940. [PubMed: 19605556]

16. Senger DR, Galli SJ, Dvorak AM, Perruzzi CA, Harvey VS, Dvorak HF. Tumor cells secrete a vascular permeability factor that promotes accumulation of ascites fluid. Science. 1983; 219:983–985. [PubMed: 6823562]

17. Antcliff RJ, Marshall J. The pathogenesis of edema in diabetic maculopathy. Semin Ophthalmol. 1999; 14:223–232. [PubMed: 10758223]

18. Fischer S, Wobben M, Marti HH, Renz D, Schaper W. Hypoxia-induced hyperpermeability in brain microvessel endothelial cells involves VEGF-mediated changes in the expression of zonula occludens-1. Microvasc Res. 2002; 63:70–80. [PubMed: 11749074]

19. Suarez S, Ballmer-Hofer K. VEGF transiently disrupts gap junctional communication in endothelial cells. Journal of Cell Science. 2001; 114:1229–1235. [PubMed: 11228166]

20. Zhu C, Barker RJ, Hunter AW, Zhang Y, Jourdan J, Gourdie RG. Quantitative analysis of ZO-1 colocalization with Cx43 gap junction plaques in cultures of rat neonatal cardiomyocytes. Microscopy and microanalysis : the official journal of Microscopy Society of America, Microbeam Analysis Society, Microscopical Society of Canada. 2005; 11:244–248.

21. Hunter AW, Jourdan J, Gourdi RG. Fusion of GFP to the Carboxyl Terminus of Connexin43 Increases Gap Junction Size in HeLa Cells. Cell Communication and Adhesion. 2003; 10:211–214. [PubMed: 14681018]

22. O'Carroll SJ, Gorrie CA, Velamoor S, Green CR, Nicholson LF. Connexin43 mimetic peptide is neuroprotective and improves function following spinal cord injury. Neuroscience research. 2013; 75:256–267. [PubMed: 23403365]

23. O'Carroll SJ, Becker DL, Davidson JO, Gunn AJ, Nicholson LF, Green CR. The use of connexin-based therapeutic approaches to target inflammatory diseases. Methods Mol Biol. 2013; 1037:519–546. [PubMed: 24029957]

24. Calder BW, Matthew Rhett J, Bainbridge H, Fann SA, Gourdie RG, Yost MJ. Inhibition of connexin 43 hemichannel-mediated ATP release attenuates early inflammation during the foreign body response. Tissue engineering Part A. 2015; 21:1752–1762. [PubMed: 25760687]

25. Palatinus JA, Rhett JM, Gourdie RG. The connexin43 carboxyl terminus and cardiac gap junction organization. Biochimica et biophysica acta. 2012; 1818:1831–1843. [PubMed: 21856279]

26. O'Quinn MP, Palatinus JA, Harris BS, Hewett KW, Gourdie RG. A Peptide Mimetic of the Connexin43 Carboxyl Terminus Reduces Gap Junction Remodeling and Induced Arrhythmia Following Ventricular Injury. Circulation Research. 2011; 108:704–715. [PubMed: 21273554]

27. Palatinus JA, Rhett JM, Gourdie RG. Enhanced PKC epsilon mediated phosphorylation of connexin43 at serine 368 by a carboxyl-terminal mimetic peptide is dependent on injury. Channels. 2011; 5:236–240. [PubMed: 21532342]

28. Ongstad EL, O'Quinn MP, Ghatnekar GS, Yost MJ, Gourdie RG. A Connexin43 Mimetic Peptide Promotes Regenerative Healing and Improves Mechanical Properties in Skin and Heart. Advances in wound care. 2013; 2:55–62. [PubMed: 24527326]
29. Ghatnekar GS, O'Quinn MP, Jourdan LJ, Gurjarpadhye AA, Draughn RL, Gourdie RG. Connexin43 carboxyl-terminal peptides reduce scar progenitor and promote regenerative healing following skin wounding. Regenerative medicine. 2009; 4:205–223. [PubMed: 19317641]
30. Rhett JM, Ghatnekar GS, Palatinus JA, O'Quinn M, Yost MJ, Gourdie RG. Novel therapies for scar reduction and regenerative healing of skin wounds. Trends Biotechnol. 2008; 26:173–180. [PubMed: 18295916]
31. Soder BL, Propst JT, Brooks TM, Goodwin RL, Friedman HI, Yost MJ, Gourdie RG. The connexin43 carboxyl-terminal peptide ACT1 modulates the biological response to silicone implants. Plastic and reconstructive surgery. 2009; 123:1440–1451. [PubMed: 19407614]
32. Grek CL, Prasad GM, Viswanathan V, Armstrong DG, Gourdie RG, Ghatnekar GS. Topical administration of a connexin43-based peptide augments healing of chronic neuropathic diabetic foot ulcers: A multicenter, randomized trial. Wound repair and regeneration : official publication of the Wound Healing Society [and] the European Tissue Repair Society. 2015; 23:203–212.
33. Ghatnekar GS, Grek CL, Armstrong DG, Desai SC, Gourdie RG. The effect of a connexin43-based Peptide on the healing of chronic venous leg ulcers: a multicenter, randomized trial. J Invest Dermatol. 2015; 135:289–298. [PubMed: 25072595]
34. Grek CL, Prasad GM, Viswanathan V, Armstrong DG, Gourdie RG, Ghatnekar GS. Topical administration of a Connexin43-based peptide augments healing of chronic neuropathic diabetic foot ulcers: A multicenter, randomized trial. Wound repair and regeneration : official publication of the Wound Healing Society [and] the European Tissue Repair Society. 2015
35. Rohrer B, Long Q, Coughlin B, Wilson RB, Huang Y, Qiao F, Tang PH, Kunchithapautham K, Gilkeson GS, Tomlinson S. A Targeted Inhibitor of the Alternative Complement Pathway Reduces Angiogenesis in a Mouse Model of Age-Related Macular Degeneration. Investigative Ophthalmology & Visual Science. 2009; 50:3056–3064. [PubMed: 19264882]
36. Kim R. Introduction, mechanism of action and rationale for anti-vascular endothelial growth factor drugs in age-related macular degeneration. Indian J Ophthalmol. 2007; 55:413–415. [PubMed: 17951895]
37. Giani A, Thanos A, Roh MI, Connolly E, Trichonas G, Kim I, Gragoudas E, Vavvas D, Miller JW. In vivo evaluation of laser-induced choroidal neovascularization using spectral-domain optical coherence tomography. Invest Ophthalmol Vis Sci. 2011; 52:3880–3887. [PubMed: 21296820]
38. Rohrer B, Long Q, Coughlin B, Wilson RB, Huang Y, Qiao F, Tang PH, Kunchithapautham K, Gilkeson GS, Tomlinson S. A targeted inhibitor of the alternative complement pathway reduces angiogenesis in a mouse model of age-related macular degeneration. Invest Ophthalmol Vis Sci. 2009; 50:3056–3064. [PubMed: 19264882]
39. Cachafeiro M, Bemelmans AP, Samardzija M, Afanasieva T, Pournaras JA, Grimm C, Kostic C, Philippe S, Wenzel A, Arsenijevic Y. Hyperactivation of retina by light in mice leads to photoreceptor cell death mediated by VEGF and retinal pigment epithelium permeability. Cell Death Dis. 2013; 4:e781. [PubMed: 23990021]
40. Strunnikova NV, Maminishkis A, Barb JJ, Wang F, Zhi C, Sergeev Y, Chen W, Edwards AO, Stambolian D, Abecasis G, et al. Transcriptome analysis and molecular signature of human retinal pigment epithelium. Hum Mol Genet. 2010; 19:2468–2486. [PubMed: 20360305]
41. Ablonczy Z, Dahrouj M, Tang PH, Liu Y, Sambamurti K, Marmorstein AD, Crosson CE. Human Retinal Pigment Epithelium Cells as Functional Models for the RPE In Vivo. Invest Ophthalmol Vis Sci. 2011; 52:8614–8620. [PubMed: 21960553]
42. Ablonczy Z, Crosson CE. VEGF modulation of retinal pigment epithelium resistance. Exp Eye Res. 2007; 85:762–771. [PubMed: 17915218]
43. Hutnik CM, Pocrnich CE, Liu H, Laird DW, Shao Q. The protective effect of functional connexin43 channels on a human epithelial cell line exposed to oxidative stress. Invest Ophthalmol Vis Sci. 2008; 49:800–806. [PubMed: 18235030]

44. Mitchell CH. Release of ATP by a human retinal pigment epithelial cell line: potential for autocrine stimulation through subretinal space. Journal of Physiology. 2001; 534:193–202. [PubMed: 11433002]
45. Peterson, Ward M., Chris, Meggyesy, Kefu, Yu, Miller, SS. Extracellular ATP Activates Calcium Signaling, Ion, and Fluid Transport in Retinal Pigment Epithelium. The Journal of Neuroscience. 1997; 17:2324–2337. [PubMed: 9065493]
46. Reigada D, Lu W, Mitchell CH. Glutamate acts at NMDA receptors on fresh bovine and on cultured human retinal pigment epithelial cells to trigger release of ATP. The Journal of physiology. 2006; 575:707–720. [PubMed: 16809361]
47. Naus CC, Aftab Q, Sin WC. Common mechanisms linking connexin43 to neural progenitor cell migration and glioma invasion. Semin Cell Dev Biol. 2016; 50:59–66. [PubMed: 26706148]
48. Matsuuchi L, Naus CC. Gap junction proteins on the move: connexins, the cytoskeleton and migration. Biochim Biophys Acta. 2013; 1828:94–108. [PubMed: 22613178]
49. Umazume K, Tsukahara R, Liu L, Fernandez de Castro JP, McDonald K, Kaplan HJ, Tamiya S. Role of retinal pigment epithelial cell beta-catenin signaling in experimental proliferative vitreoretinopathy. Am J Pathol. 2014; 184:1419–1428. [PubMed: 24656918]
50. Zhang XG, Hui YN, Huang XF, Du HJ, Zhou J, Ma JX. Activation of formyl peptide receptor-1 enhances restitution of human retinal pigment epithelial cell monolayer under electric fields. Invest Ophthalmol Vis Sci. 2011; 52:3160–3165. [PubMed: 21228377]
51. Rothen-Rutishauser B, Riesen FK, Braun A, Gunthert M, Wunderli-Allenspach H. Dynamics of tight and adherens junctions under EGTA treatment. J Membr Biol. 2002; 188:151–162. [PubMed: 12172640]
52. Ehmann UK, Calderwood SK, Stevenson MA. Gap-junctional communication between feeder cells and recipient normal epithelial cells correlates with growth stimulation. In vitro cellular & developmental biology Animal. 2001; 37:100–110. [PubMed: 11332735]
53. Gaudana R, Ananthula HK, Parenky A, Mitra AK. Ocular drug delivery. AAPS J. 2010; 12:348–360. [PubMed: 20437123]
54. Cheruvu NP, Amrite AC, Kompella UB. Effect of eye pigmentation on transscleral drug delivery. Invest Ophthalmol Vis Sci. 2008; 49:333–341. [PubMed: 18172110]
55. Campa C, Kasman I, Ye W, Lee WP, Fuh G, Ferrara N. Effects of an anti-VEGF-A monoclonal antibody on laser-induced choroidal neovascularization in mice: optimizing methods to quantify vascular changes. Invest Ophthalmol Vis Sci. 2008; 49:1178–1183. [PubMed: 18326747]
56. Murakami T, Felinski EA, Antonetti DA. Occludin phosphorylation and ubiquitination regulate tight junction trafficking and vascular endothelial growth factor-induced permeability. The Journal of biological chemistry. 2009; 284:21036–21046. [PubMed: 19478092]
57. Rao R. Occludin phosphorylation in regulation of epithelial tight junctions. Ann N Y Acad Sci. 2009; 1165:62–68. [PubMed: 19538289]
58. Peng S, Rao VS, Adelman RA, Rizzolo LJ. Claudin-19 and the barrier properties of the human retinal pigment epithelium. Invest Ophthalmol Vis Sci. 2011; 52:1392–1403. [PubMed: 21071746]
59. Xu H, Liversidge J. Quantitative in situ analysis of claudin expression at the blood-retinal barrier. Methods Mol Biol. 2011; 762:321–331. [PubMed: 21717367]
60. Schnabolk G, Coughlin B, Joseph K, Kunchithapautham K, Bandyopadhyay M, O'Quinn EC, Nowling T, Rohrer B. Local production of the alternative pathway component factor B is sufficient to promote laser-induced choroidal neovascularization. Invest Ophthalmol Vis Sci. 2015; 56:1850–1863. [PubMed: 25593023]
61. Gunduz D, Aslam M, Krieger U, Becker L, Grebe M, Arshad M, Sedding DG, Hartel FV, Abdallah Y, Piper HM, et al. Opposing effects of ATP and adenosine on barrier function of rat coronary microvasculature. Journal of molecular and cellular cardiology. 2012; 52:962–970. [PubMed: 22266063]
62. Block ER, Klarlund JK. Wounding sheets of epithelial cells activates the epidermal growth factor receptor through distinct short- and long-range mechanisms. Mol Biol Cell. 2008; 19:4909–4917. [PubMed: 18799627]
63. Rizzolo LJ. Development and role of tight junctions in the retinal pigment epithelium. Int Rev Cytol. 2007; 258:195–234. [PubMed: 17338922]

64. Balcarova-Stander J, Pfeiffer SE, Fuller SD, Simons K. Development of cell surface polarity in the epithelial Madin-Darby canine kidney (MDCK) cell line. EMBO J. 1984; 3:2687–2694. [PubMed: 6391916]

65. Zhang Y, Yeh S, Appleton BA, Held HA, Kausalya PJ, Phua DC, Wong WL, Lasky LA, Wiesmann C, Hunziker W, et al. Convergent and divergent ligand specificity among PDZ domains of the LAP and zonula occludens (ZO) families. J Biol Chem. 2006; 281:22299–22311. [PubMed: 16737968]

66. Utepbergenov DI, Fanning AS, Anderson JM. Dimerization of the scaffolding protein ZO-1 through the second PDZ domain. J Biol Chem. 2006; 281:24671–24677. [PubMed: 16790439]

67. Wu J, Yang Y, Zhang J, Ji P, Du W, Jiang P, Xie D, Huang H, Wu M, Zhang G, et al. Domain-swapped dimerization of the second PDZ domain of ZO2 may provide a structural basis for the polymerization of claudins. J Biol Chem. 2007; 282:35988–35999. [PubMed: 17897942]

68. Rodgers LS, Beam MT, Anderson JM, Fanning AS. Epithelial barrier assembly requires coordinated activity of multiple domains of the tight junction protein ZO-1. J Cell Sci. 2013; 126:1565–1575. [PubMed: 23418357]

69. Chen J, Pan L, Wei Z, Zhao Y, Zhang M. Domain-swapped dimerization of ZO-1 PDZ2 generates specific and regulatory connexin43-binding sites. EMBO J. 2008; 27:2113–2123. [PubMed: 18636092]

70. Burnstock G. Purinergic signalling. British journal of pharmacology. 2006; 147(Suppl 1):S172–S181. [PubMed: 16402102]

71. Contreras JE, Saez JC, Bukauskas FF, Bennett MV. Gating and regulation of connexin 43 (Cx43) hemichannels. Proceedings of the National Academy of Sciences of the United States of America. 2003; 100:11388–11393. [PubMed: 13130072]

72. Morita M, Saruta C, Kozuka N, Okubo Y, Itakura M, Takahashi M, Kudo Y. Dual regulation of astrocyte gap junction hemichannels by growth factors and a pro-inflammatory cytokine via the mitogen-activated protein kinase cascade. Glia. 2007; 55:508–515. [PubMed: 17211868]

73. Ozaki E, Campbell M, Kiang AS, Humphries M, Doyle SL, Humphries P. Inflammation in age-related macular degeneration. Adv Exp Med Biol. 2014; 801:229–235. [PubMed: 24664703]

74. Rutar M, Natoli R, Chia RX, Valter K, Provis JM. Chemokine-mediated inflammation in the degenerating retina is coordinated by Muller cells, activated microglia, and retinal pigment epithelium. J Neuroinflammation. 2015; 12:8. [PubMed: 25595590]

75. Guo CX, Tran H, Green CR, Danesh-Meyer HV, Acosta ML. Gap junction proteins in the light-damaged albino rat. Mol Vis. 2014; 20:670–682. [PubMed: 24883012]

76. Ghatnekar GS, O'Quinn PM, Jourdan JL, Gurjarpadhye AARL, Draughn RL, Gourdie RG. Connexin43 carboxyl- terminal peptides reduce scar progenitor and promote regenerative healing following skin wounding. Regenerative Medicine. 2009; 4:205–223. [PubMed: 19317641]

77. Soder BL, Propst JT, Brooks TM, Friedman HI, Goodwin RLMJ, Y RGG. The Cx43 carboxyl terminal peptide ACT1 modulates the biological response to silicone implants. Journal of Plastic and Reconstructive Surgery. 2009; 123:1440–1451. [PubMed: 19407614]

78. Moore K, Amos J, Davis J, Gourdie R, Potts JD. Characterization of polymeric microcapsules containing a low molecular weight peptide for controlled release. Microsc Microanal. 2013; 19:213–226. [PubMed: 23360728]

79. Machalinska A, Safranow K, Mozolewska-Piotrowska K, Dziedziejko V, Karczewicz D. PEDF and VEGF plasma level alterations in patients with dry form of age-related degeneration--a possible link to the development of the disease. Klin Oczna. 2012; 114:115–120. [PubMed: 23346798]

80. Schutze C, Wedl M, Baumann B, Pircher M, Hitzenberger CK, Schmidt-Erfurth U. Progression of retinal pigment epithelial atrophy in antiangiogenic therapy of neovascular age-related macular degeneration. Am J Ophthalmol. 2015; 159:1100–1114. e1101. [PubMed: 25769245]

81. Ranjbar M, Brinkmann MP, Tura A, Rudolf M, Miura Y, Grisanti S. Ranibizumab interacts with the VEGF-A/VEGFR-2 signaling pathway in human RPE cells at different levels. Cytokine. 2016; 83:210–216. [PubMed: 27163716]

82. Kurihara T, Westenskow PD, Bravo S, Aguilar E, Friedlander M. Targeted deletion of Vegfa in adult mice induces vision loss. J Clin Invest. 2012; 122:4213–4217. [PubMed: 23093773]

83. Nozaki M, Raisler BJ, Sakurai E, Sarma JV, Barnum SR, Lambris JD, Chen Y, Zhang K, Ambati BK, Baffi JZ, et al. Drusen complement components C3a and C5a promote choroidal

neovascularization. Proceedings of the National Academy of Sciences of the United States of America. 2006; 103:2328–2333. [PubMed: 16452172]

84. Giani A, Thanos A, Roh MI, Connolly E, Trichonas G, Kim I, Gragoudas E, Vavvas D, Miller JW. In Vivo Evaluation of Laser-Induced Choroidal Neovascularization Using Spectral-Domain Optical Coherence Tomography. Investigative Ophthalmology & Visual Science. 2011; 52:3880–3887. [PubMed: 21296820]
85. Nozaki M, Raisler BJ, Sakurai E, Sarma JV, Barnum SR, Lambris JD, Chen Y, Zhang K, Ambati BK, Baffi JZ, et al. Drusen complement components C3a and C5a promote choroidal neovascularization. Proc Natl Acad Sci USA. 2006; 103:2328–2333. [PubMed: 16452172]
86. Jeffrey, Gresh, Goletz, Patrice W., Crouch, Rosalie K., Rohrer, B. Structure–function analysis of rods and cones in juvenile, adult, and aged C57BL06 and Balb0c mice. 2003:20.
87. Adam, Richards, Alfred, A., Emondi, J., Rohrer, B. Long-term ERG analysis in the partially light-damaged mouse retina reveals regressive and compensatory changes. Visual Neuroscience. 2006; 23:91–97. [PubMed: 16597353]
88. Narimatsu T, Ozawa Y, Miyake S, Kubota S, Hirasawa M, Nagai N, Shimmura S, Tsubota K. Disruption of Cell-Cell Junctions and Induction of Pathological Cytokines in the Retinal Pigment Epithelium of Light-Exposed Mice. Investigative Ophthalmology & Visual Science. 2013; 54:4555–4562. [PubMed: 23761083]
89. Thurman JM, Renner B, Kunchithapautham K, Ferreira VP, Pangburn MK, Ablonczy Z, Tomlinson S, Holers VM, Rohrer B. Oxidative Stress Renders Retinal Pigment Epithelial Cells Susceptible to Complement-mediated Injury. Journal of Biological Chemistry. 2009; 284:16939–16947. [PubMed: 19386604]
90. Thurman JM, Renner B, Kunchithapautham K, Ferreira VP, Pangburn MK, Ablonczy Z, Tomlinson S, Holers VM, Rohrer B. Oxidative stress renders retinal pigment epithelial cells susceptible to complement-mediated injury. J Biol Chem. 2009; 284:16939–16947. [PubMed: 19386604]
91. Fernandez-Godino R, Garland DL, Pierce EA. Isolation, culture and characterization of primary mouse RPE cells. Nat Protoc. 2016; 11:1206–1218. [PubMed: 27281648]
92. Schlegel N, Meir M, Heupel WM, Holthofer B, Leube RE, Waschke J. Desmoglein 2-mediated adhesion is required for intestinal epithelial barrier integrity. Am J Physiol Gastrointest Liver Physiol. 2010; 298:G774–G783. [PubMed: 20224006]
93. Sidhaye VK, Chau E, Breysse PN, King LS. Septin-2 mediates airway epithelial barrier function in physiologic and pathologic conditions. Am J Respir Cell Mol Biol. 2011; 45:120–126. [PubMed: 20870893]

KEY MESSAGES

- The connexin43 mimetic αCT1 accumulates in the mouse retinal pigment epithelium following topical delivery via eye drops.
- αCT1 eye drops prevented RPE-cell barrier dysfunction in two mouse models.
- αCT1 stabilizes intercellular tight junctions.
- Stabilization of cellular junctions via αCT1 may serve as a novel therapeutic approach for both wet and dry age-related macular degeneration.

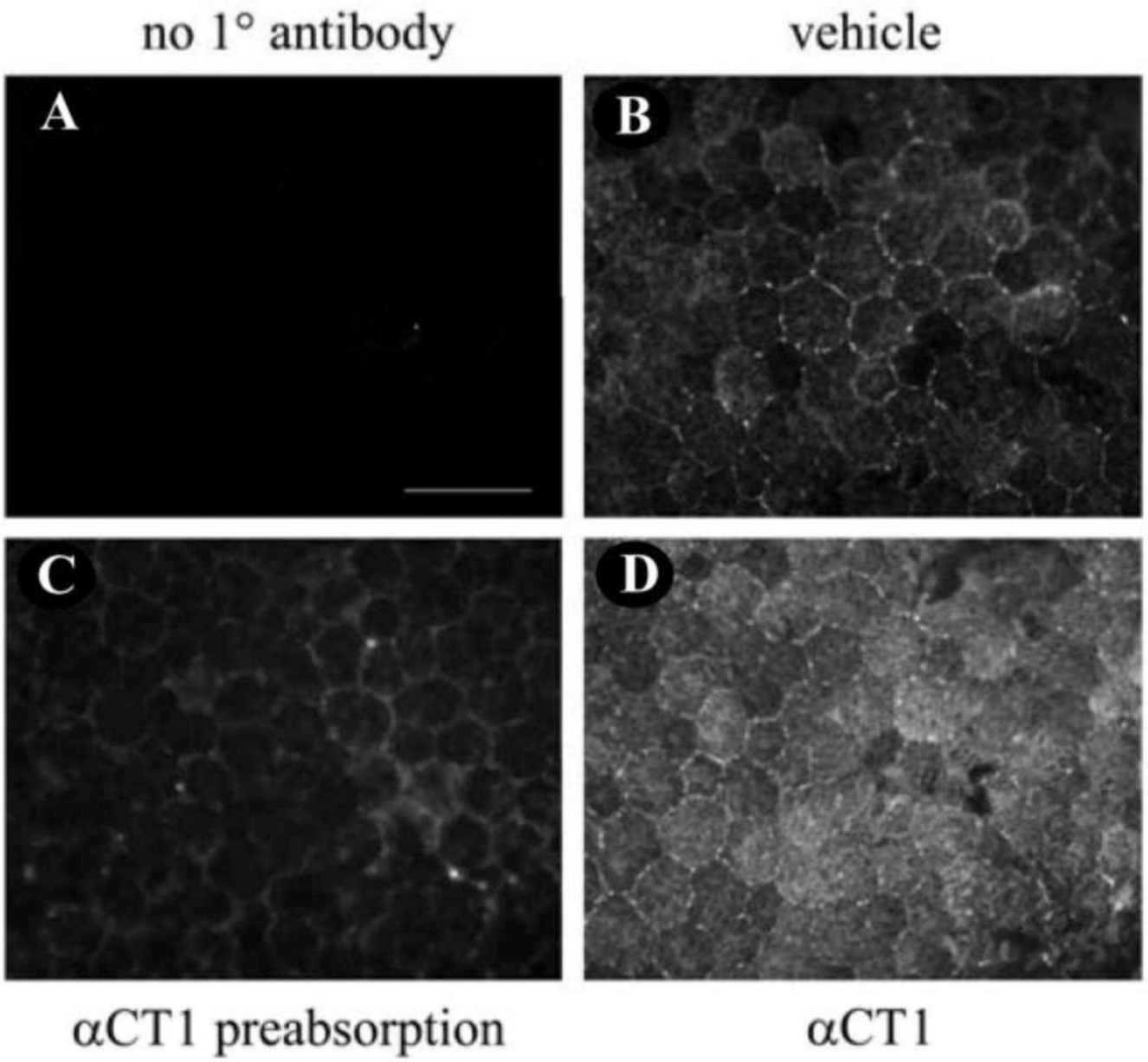

Figure 1. αCT1 detection in murine RPE flatmounts

The αCT1 peptide has an amino acid sequence that is a mimetic of the Cx43 C-terminal sequence. Thus, the peptide can be detected via a Cx43 antibody that recognizes the C-terminal domain. The eyes of the mouse that received the peptide were enucleated 4 hours after eye drop administration and stained for Cx43. The αCT1 peptide could be clearly detected in the animal that received the treatment drops (**D**), when compared to vehicle-treated animals (**B**). No primary antibody (**A**) and antibody preabsorption with 10× molar excess of peptide (**C**) were used as controls. Scale bar: 50 μm.

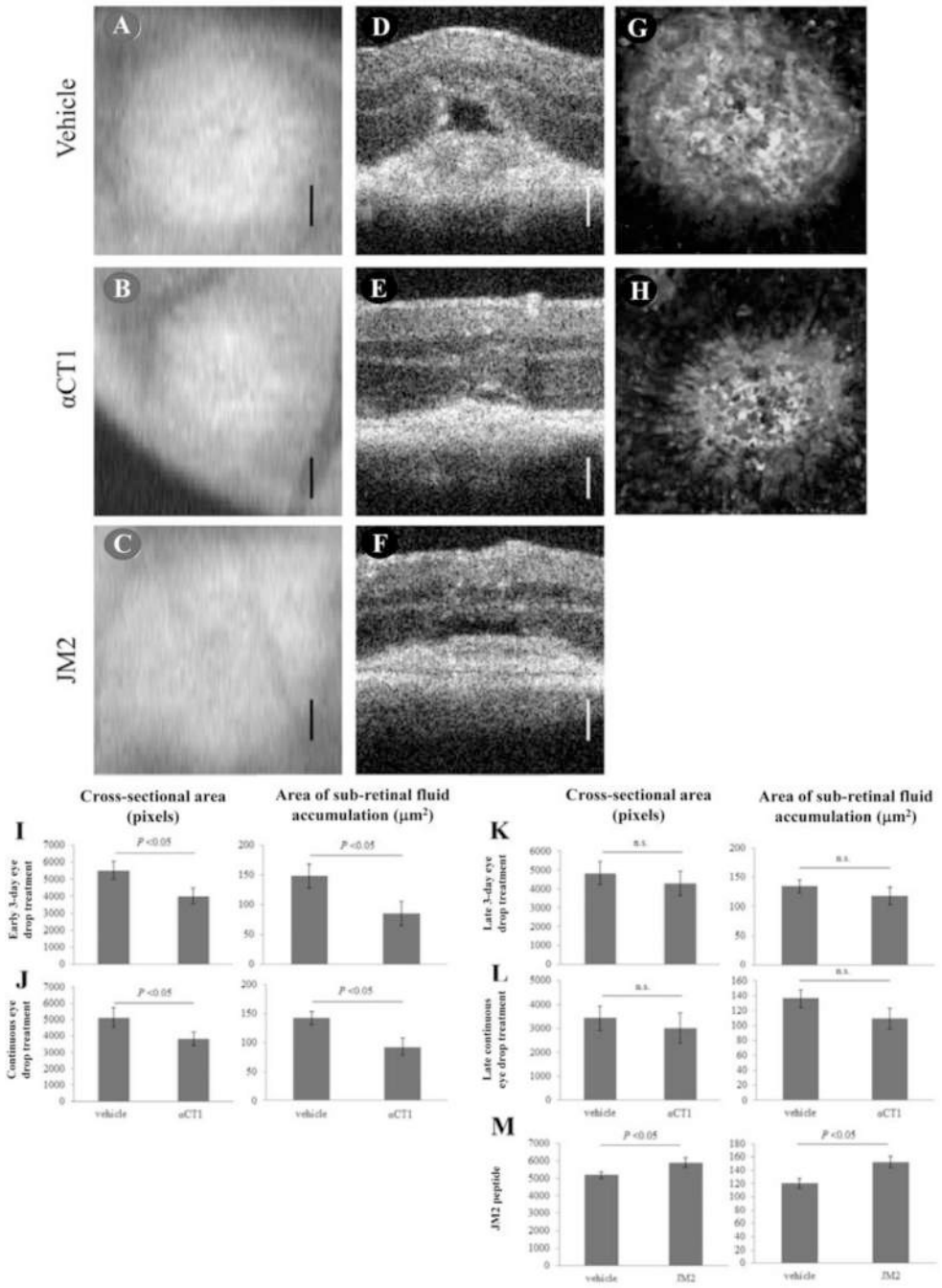

Figure 2. Choroidal neovascularization and fluid leakage in αCT1- versus vehicle-treated mice

Animals were analyzed post laser-photocoagulation by SD-OCT. The cross-sectional area of the hyporeflective spot seen in the fundus image (**A–C**) as well as the area of fluid accumulation in the outer retina (**D–F**) were determined and representative OCT images taken from the vehicle (**A, D**), αCT1-treated (**B, E**) and JM2-treated animals (**C, F**) are depicted. CNV area and fluid accumulation were determined from SD-OCT images. Quantifications of the cross-sectional areas of the lesions (**I–M, left-hand column**) as well as areas of fluid accumulation (**I–M, right-hand column**) were measured in pixels for the

individual treatment groups. CNV size and area of fluid accumulation in αCT1-treated animals was significantly reduced, compared to the vehicle group for the continuous (**J**) and early (**I**) treatment paradigms. No significance was noted between the vehicle and the two groups for the late αCT1 treatment study (**K, L**). Angiogenesis was confirmed in flat-mount preparations of RPE-choroid stained with isolectin B, with αCT1significantly reducing the size of the lesion (**H**) when compared to control (**G**). (**K**) JM2-treatment, a Cx43 peptide that includes the microtubule-binding sequence and targets hemichannels, resulted in an increase in CNV size and area of fluid accumulation. Data are expressed as mean ± SEM (n = 7–23 animals per treatment group). Scale bar: 100 pixels or 160 μm.

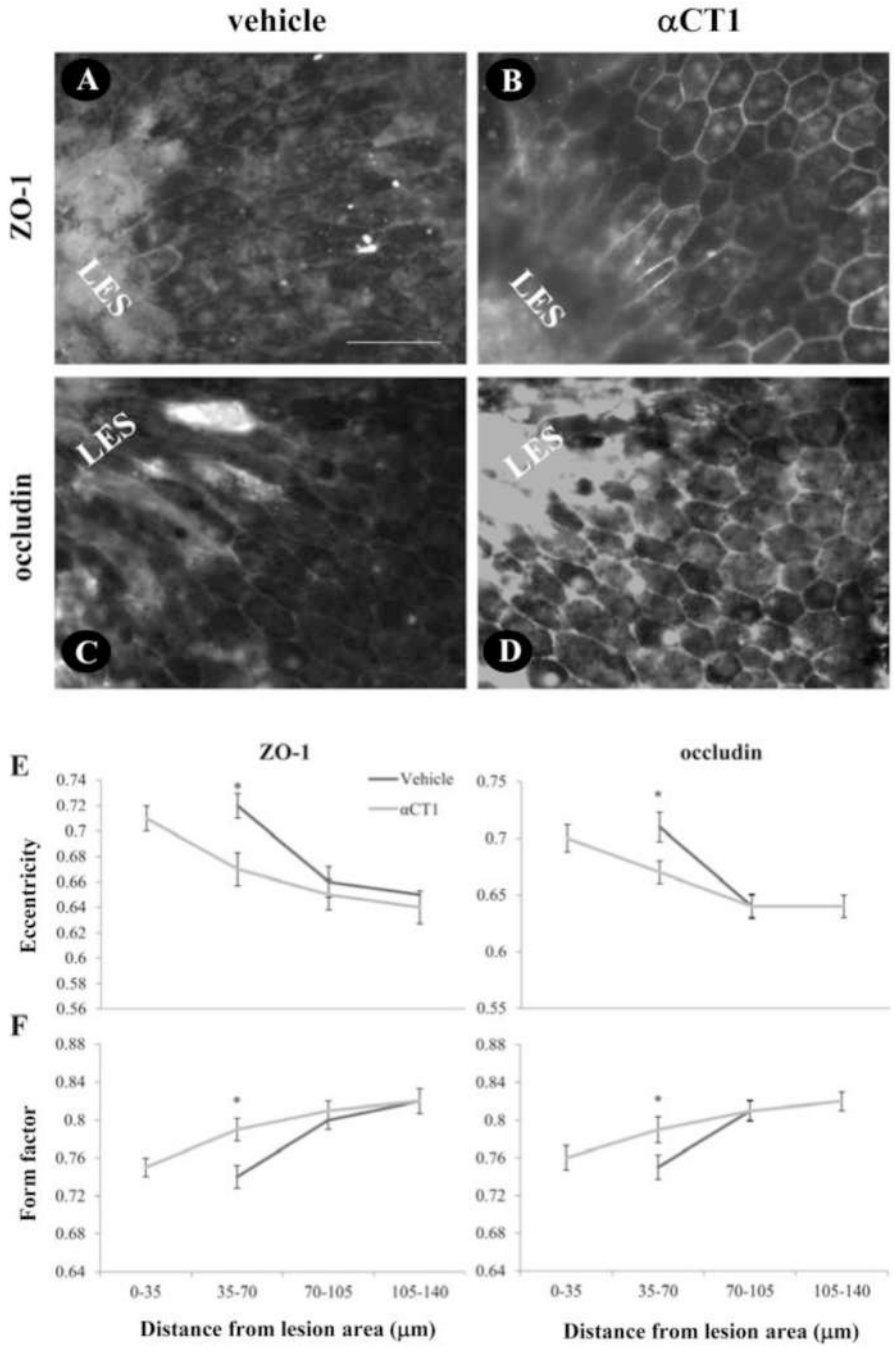

Figure 3. RPE integrity in αCT1 compared to vehicle-treated mice

On day 6 after the induction of CNV, eyes were enucleated and RPE/choroid eyecups were stained for two different cell junction markers, ZO-1 (**A, B**) and occludin (**C, D**). Representative images for each cell junction marker are presented, depicting the differences in the diameter of unhealthy cells (peri-lesion area) surrounding the lesion (LES) in the control group compared to the αCT1-treated animals. Morphometric analyses were obtained from images as depicted in Figure 2, comparing two measures of RPE cell shape, cell eccentricity (**E**) and form factor (**F**) in 4 steps of 35 μm each (bins 1–4) for both ZO-1 (**left-**

hand column) and occludin (**right-hand column**). Cell eccentricity measures the deviation of a shape from an ellipse; form factor measures the deviation from a perfect circle. RPE cells from C57BL/6J mice exhibit a form factor of ~0.82 and an eccentricity value of ~0.65. RPE cells from animals treated with the αCT1 peptide exhibited form factor and eccentricity values closer to normal, closer to the edge of the lesions when compared to mice treated with vehicle. Data are expressed as mean ± SEM (n = 7–8 animals per cell junction marker). Scale bar: 50 μm.

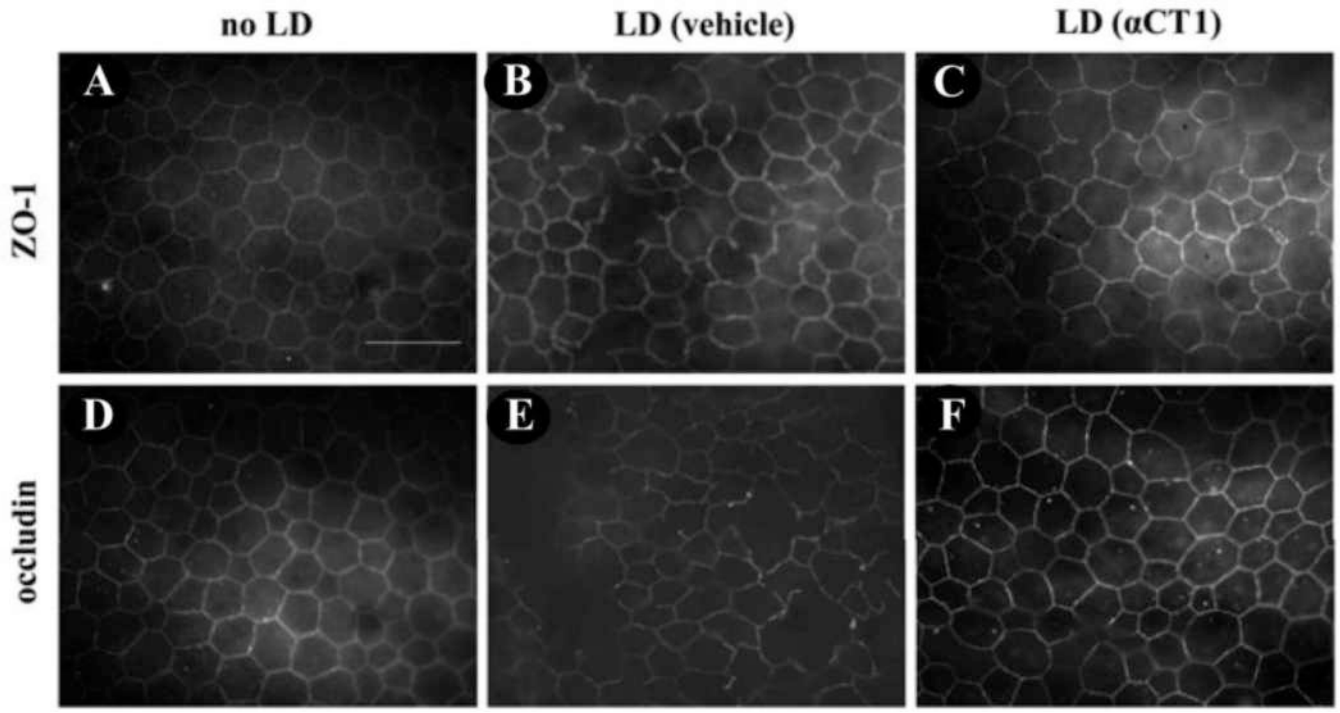

Figure 4. RPE morphology following light-damage

Balb/c mice were exposed to bright light (3000 lux) for 3 hours, sacrificed and eyes enucleated after 24 hours. RPE morphology was analyzed by immunohistochemistry for ZO-1 (**A–C**) and occludin (**D–F**) on RPE/choroid flatmounts from the respective treatment groups, no light damage controls (**A, D**), light damage treated with vehicle (**B, E**) and light damage treated with αCT1 peptide (**C, F**). Scale bar: 50 μm.

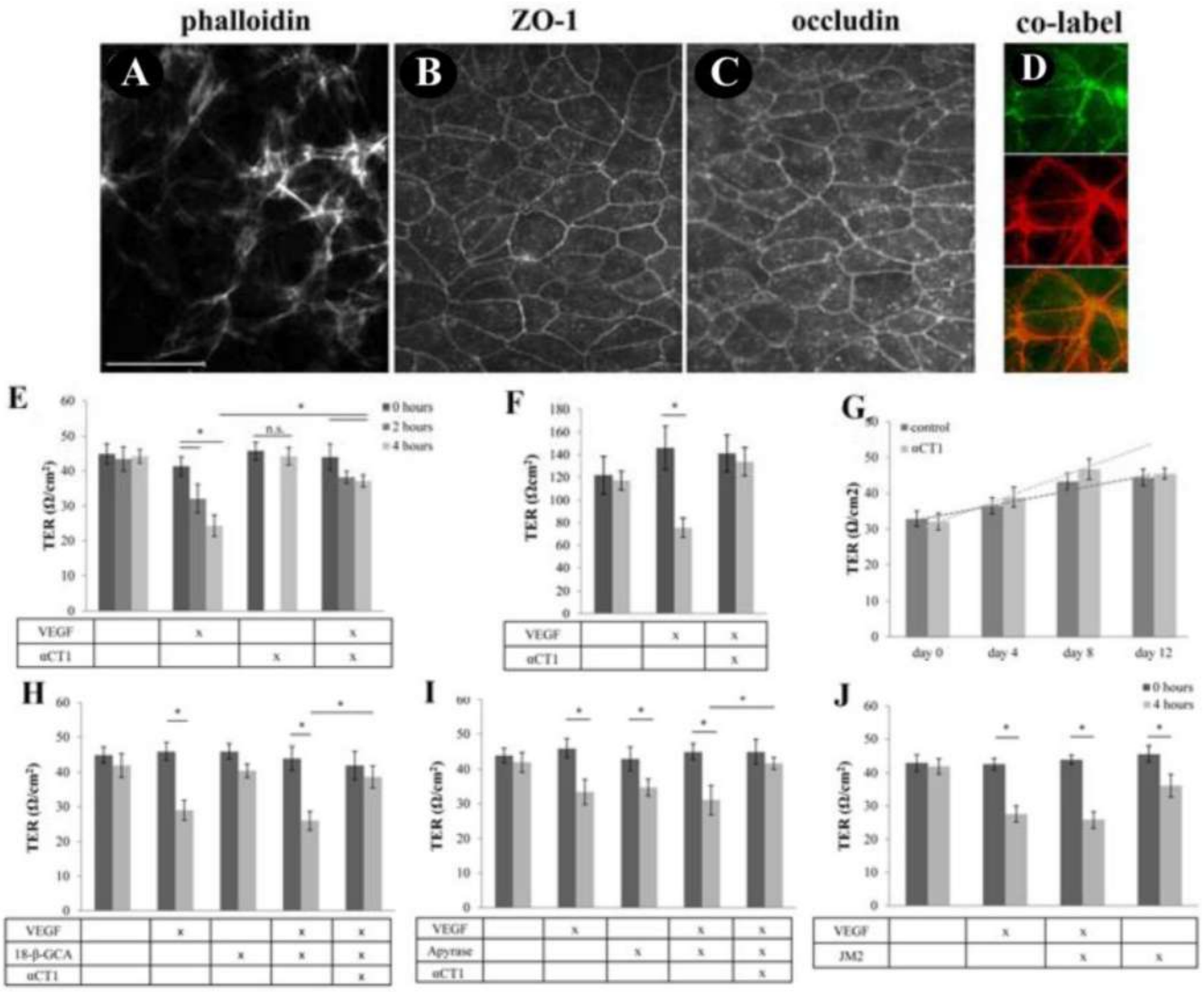

Figure 5. Effects of αCT1 on VEGF-mediated loss in barrier function; analysis of mechanism of action

ARPE-19 and primary mouse RPE cells were grown on Transwell plates for >3 weeks after which they formed a monolayer with stable transepithelial resistance (TER). TER was measured via a volt-ohm meter with an STX2 electrode. The integrity of the monolayer was confirmed in ARPE-19 cells, demonstrating the presence of β-actin filament distribution in the form of circumferential bundles (**A**), cell-junction markers at the cell-borders, ZO-1 (**B**) and occludin (**C**), and co-labeling of ZO-1 and phalloidin (**D**). (**E**) In ARPE-19 cells, VEGF (10 ng/mL) significantly (P <0.05) reduced TER by 2 and 4 hours post-application. Pretreatment with 100 μM αCT1 ameliorated the drop in TER at both time points. αCT1 alone had no effect over the four hour time course. (**F**) The protective effect of αCT1 was confirmed in RPE monolayers derived from mouse. (**G**) Treatment of the ARPE-19 cell monolayers for 12 days starting at confluency (day 0) resulted in higher TER levels in the αCT1 when compared to the control group (P =0.03), reaching maximal TER levels 4 days earlier (indicated by the slope). (**H**) The gap-junction blocker, 18-β-GCA (0.1 mM), did not

reduce the protective effect of αCT in ARPE-19 cells, neither did two modulators of hemichannels, apyrase and JM2 as shown by TER measurements at the 4 hour time point (**I, J**). Data are expressed as mean ± SD for ARPE-19 cells, mean ± SEM for primary mouse RPE cells (n = 3 per treatment group). Scale bar: 50 μm.

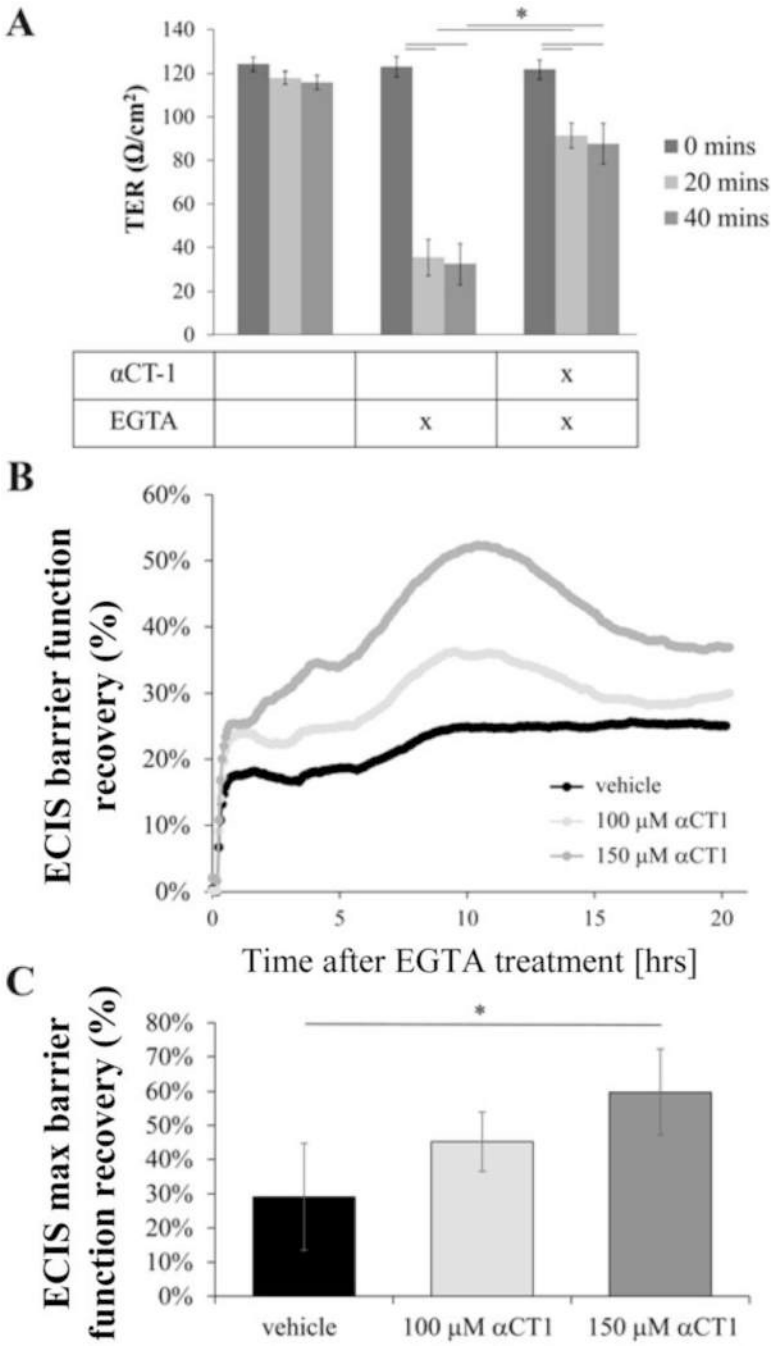

Figure 6. Effects of αCT1 on calcium-chelation-mediated loss in barrier function of MDCK cells

Barrier function was measured in MDCK cells in response to calcium chelation during the damage phase (transepithelial resistance measurements [TER] using a volt-ohm meter with an STX2 electrode) or during the recovery phase (Electric Cell-Substrate Impedance Sensing [ECIS] system). (**A**) MDCK cells were grown in Transwell plates for >3 weeks to measure barrier function by TER. Measurements were obtained at baseline and 20 and 40 minutes after the addition of 1.2 mM EGTA in αCT1-pretreated (30 μM) and untreated cells. EGTA treatment decreased barrier function within 20 minutes; but significantly less so in the

αCT1 group. Data are expressed as mean ± SEM (n = 6 per treatment group). (**B**) MDCK cells grown in 8W10E+ ECIS dishes were used to measure barrier function using an ECIS system. Impedence was measured at baseline, after the addition of 0.5 mM EGTA and during the recovery phase upon restoration of physiological levels of calcium, in αCT1- and untreated cells. Calcium chelation significantly decreased barrier function, which recovered upon re-addition of calcium. Revovery of impendance was expressed as the rate of barrier function following EGTA treatment to the mean barrier function at 1 hour after αCT1 or vehicle treatment (**C**). Recovery was significantly accelerated in αCT1- when compared to un-treated cells Data are expressed as mean ± SEM (n = 6–8 per treatment group).

Table 1

Morphometric analyses to quantify changes in retinal pigment epithelium cells in ZO-1- and Occludin-stained images using CellProfiler

	Mean values of:	no LD	LD Vehicle	LD αCT1
ZO1	Cell count	60 ±2	44 ±5 *	56 ±3
	Form factor	0.82 ±0.02	0.76 ±0.04 *	0.79 ±0.03
	Eccentricity	0.64 ±0.01	0.69 ±0.02 *	0.65 ±0.01
	Number of neighbors	5.7 ±0.8	4.3 ±1.3 *	5.4 ±1.1
	Perimeter	79 ±4	52 ±8 *	71 ±6
	Area covered	96 ±9	62 ±13 *	93 ±10
Occludin	Cell count	63 ±3	48 ±7 *	59 ±2
	Form factor	0.79 ±0.02	0.71 ±0.03 *	0.77 ±0.04
	Eccentricity	0.62 ±0.01	0.68 ±0.02 *	0.64 ±0.02
	Number of neighbors	5.8 ±0.7	4.1 ±0.9 *	5.6 ±0.8
	Perimeter	76 ±6	49 ±12 *	69 ±8
	Area covered (%)	95 ±7	64 ±9 *	91 ±8

Measurements were significant (* $P<0.05$) between the no light damage controls (no LD) and the light-damaged PBS-treated animals (LD vehicle) for all morphometric factors analyzed. No significance in morphometric measurements were identified between light-exposed animals that were treated with αCT1 (LD αCT1) and subjects that were never exposed to bright light (no LD, control).

LD, light damage; vehicle, phosphate-buffered saline; αCT1, connexin-based peptide mimetic

Table 2

Morphometric analysis to quantify changes in retinal pigment epithelium cells in ZO-1-stained images using CellProfiler to determine the therapeutic window for αCT1.

Mean values of:	no LD	LD vehicle	LD αCT1 (−4 hour)	LD αCT1 (−2 hour)	LD αCT1 (−1 hour)	LD αCT1 (+1 hour)	LD αCT1 (+4 and +6 hours)
Cell Count	62 ±3	42 ±5	57 ±2 *	54 ±5	50 ±4	52 ±3	46 ±4
Form Factor	0.81 ±0.02	0.75 ±0.02	0.79 ±0.01 *	0.78 ±0.02 *	0.77 ±0.03	0.75 ±0.02	0.76 ±0.03
Eccentricity	0.63 ±0.01	0.71 ±0.01	0.66 ±0.1 *	0.67 ±0.03 *	0.65 ±0.01 *	0.69 ±0.03	0.7 ±0.02
Number of Neighbors	5.8 ±0.7	4.3 ±0.6	5.2 ±1.2	5.3 ±0.7 *	5.4 ±1.3 *	4.7 ±0.8	4.5 ±0.9
Perimeter	76 ±4	53 ±6	69 ±4 *	72 ±5 *	73 ±5 *	65 ±8	51 ±11
Area Covered (%)	97 ±6	64 ±8	92 ±2 *	88 ±4 *	91 ±3 *	73 ±11	60 ±10

Animals were treated at the indicated times (−4, −2, −1, +1, +4 and +6 hours) with zero representing the time of Light ON. Protection was identified (i.e, measurements were significant; * $P<0.05$) for the majority of morphometric factors analyzed for the treatment groups that initiated treatment prior to the onset of light damage.

LD, light damage; vehicle, phosphate-buffered saline; αCT1, connexin-based peptide mimetic